Processes controlling highly siderophile element fractionations in xenolithic peridotites and their influence on Os isotopes

Jingao Liu [a,*], Roberta L. Rudnick [a], Richard J. Walker [a], Shan Gao [b], Fuyuan Wu [c], Philip M. Piccoli [a]

[a] Department of Geology, University of Maryland, College Park, MD 20742, USA
[b] Faculty of Earth Science, China University of Geosciences, Wuhan 430074, China
[c] State Key Laboratory of Lithospheric Evolution, Institute of Geology and Geophysics, Chinese Academy of Sciences, P.O. Box 9825, Beijing 100029, China

ARTICLE INFO

ABSTRACT

Xenolithic peridotites having a similar range of major element compositions from two nearby localities in the Trans-North China Orogen, North China Craton, provide a rare opportunity to explore effects resulting from both primary partial melting and secondary processes on Os isotopes and highly siderophile element (HSE) abundances. HSE patterns of peridotites from Hannuoba are similar to those of orogenic peridotite massifs worldwide, but are rare for xenolithic peridotites. These patterns can be explained by relatively low degrees of melt depletion, coupled with long-term preservation of sulfides. By contrast, peridotites from Yangyuan have major element compositions similar to or slightly more depleted than Hannuoba xenoliths, but are characterized by distinct, highly fractionated HSE patterns with lower total HSE abundances and Os, Pd and Re depletions relative to Ir. Some of the latter HSE characteristics must reflect secondary processes. The low S and Se contents of Yangyuan peridotites, coupled with scarcity of observable sulfides, suggest that they experienced sulfide breakdown, possibly as a result of interaction with a S-undersaturated melt/fluid. This may have occurred under oxidizing conditions, as suggested by the somewhat higher fO_2 recorded in the Yangyuan peridotites compared to the Hannuoba peridotites, as well as the metal-deficient composition of rare, mono-sulfide-solid solution (mss) sulfides within the Yangyuan peridotites. We speculate that under such conditions, Os, Pd, and possibly Re, more strongly partition into a sulfide liquid, or the oxidizing medium (melt or fluid), than Ir and Pt and, thus, become depleted. These effects would have been imposed on original patterns that were similar to those in the Hannuoba suite. The good correlation between $^{187}Os/^{188}Os$ and major element indices of melt depletion in the Yangyuan rocks, coupled with the poor correlation between $^{187}Os/^{188}Os$ and $^{187}Re/^{188}Os$, suggests that the S, Os, Pd and Re removal was recent. Hence, the long-term Re–Os isotopic systematics of these rocks would not have been affected, and Re depletion model ages, based on Os isotopes, remain viable to constrain the timing of melt deletion in these peridotites. The similarity of model age distributions between Yangyuan and Hannuoba peridotites ($T_{RD} = 0$ to 1.7 and 0 to 1.5 Ga, respectively) is consistent with this, and further indicates that these peridotites formed in the Paleoproterozoic.

© 2010 Elsevier B.V. All rights reserved.

1. Introduction

Highly siderophile element (HSE, including Os, Ir, Ru, Pt, Pd and Re) abundances of mantle rocks are important in tracing the Earth's core–mantle segregation, late accretion, and mantle differentiation (e.g., Morgan et al., 2001). Further, the $^{187}Re–^{187}Os$ isotopic system provides a potential means to date formation of lithospheric mantle (e.g., Walker et al., 1989). Unlike lithophile elements in mantle peridotites, HSE dominantly reside in trace phases, such as sulfides and alloys, rather than major phases (e.g., Hart and Ravizza, 1996; Alard et al., 2000; Bockrath et al., 2004; Lorand et al., 2008a, 2010).

During partial melting of the mantle, base metal sulfides that concentrate Re, Pt and Pd may preferentially enter the melt phase relative to more refractory sulfides, such as monosulfide solid solution (mss), and alloys that sequester Os, Ir and Ru (e.g., Alard et al., 2000; Luguet et al., 2003; 2007). This division of HSE into sulfides with distinct melting characteristics, along with possible molten sulfide entrained into melts (Bockrath et al., 2004; Ballhaus et al., 2006), can lead to depletions of Re and platinum-like platinum group elements (PPGE: Pd and Pt), relative to iridium-like platinum group elements (IPGE: Os, Ir and Ru), as long as mss remains in the residue (e.g., Pearson et al., 2004). In addition to partial melting, mantle peridotites might also undergo secondary processes (i.e., all processes postdating partial melting), such as refertilization (addition of melt) (e.g., Elthon, 1992; Saal et al., 2001; Le Roux et al., 2007), mantle metasomatism via melt–rock reaction (Büchl et al., 2002; Ackerman et al., 2009), and

* Corresponding author. Department of Geology, University of Maryland, College Park, MD 20742 USA.
E-mail address: gobyliu@geol.umd.edu (J. Liu).

sulfide breakdown, a general term used to describe several possible processes associated with sulfur loss (e.g., Handler et al., 1999; Handler and Bennett, 1999; Lorand et al., 2003a). Secondary processes may strongly modify HSE abundances of peridotites, e.g., Os loss relative to Ir (Handler et al., 1999), and also potentially affect their Re–Os isotopic systematics (e.g., Büchl et al., 2002).

Here, we report on two suites of xenolithic peridotites from nearby areas in China that have largely similar major element compositions but distinct HSE patterns. These suites provide an unusual opportunity to explore primary and secondary processes that may act on HSE contained within mantle peridotites and assess the impacts of these processes on Os isotope and HSE systematics.

2. Samples

The xenoliths studied here are anhydrous spinel peridotites entrained in Tertiary basaltic lavas from the Hannuoba and Yangyuan areas in the northern part of the Trans-North China Orogen, North China Craton (see Fig. 1 in Y.G. Xu et al., 2008). These two localities lie approximately 100 km apart. The Hannuoba basalts erupted between 14 and 24 Ma ago (Liu et al., 1992) and consist of interlayered alkali and tholeiitic basalt (Zhi et al, 1990); the Damaping lavas, which host the xenoliths studied here, are alkali basalts. The Yangyuan basalts erupted 30–35 Ma ago (Liu et al., 1992) and mainly consist of alkali basalts (Ma and Xu, 2004).

Petrologic and geochemical characteristics of peridotite xenoliths from these localities were previously documented in Song and Frey (1989) and Rudnick et al. (2004) for Hannuoba, and Y.G. Xu et al. (2008) for Yangyuan. Both peridotite suites are dominated by protogranular to equigranular spinel lherzolites, but also contain a small proportion of harzburgites (Rudnick et al., 2004; Y.G. Xu et al., 2008). While both suites are generally fresh, the Hannuoba peridotites typically contain grain boundary serpentine, while the Yangyuan peridotites do not.

The Hannuoba samples considered here were previously analyzed for major elements, sulfur and Re–Os isotopes by Gao et al. (2002), for mineral chemistry, lithophile trace elements and Sr–Nd isotopes by Rudnick et al. (2004), and for HSE and reanalysis of Re–Os isotopes by Becker et al. (2006). In addition, we have analyzed the HSE and re-analyzed Re–Os isotopes in an additional Hannuoba sample from the Gao et al. (2002) study, as well as a subset of Hannuoba peridotites recently investigated by Zhang et al. (2009).

The Yangyuan samples investigated here are from a new collection that has not been previously studied. In addition, we have analyzed the HSE and re-analyzed Re–Os isotopes in a subset of Yangyuan peridotites recently investigated by Y.G. Xu et al. (2008), who also reported whole rock major and lithophile trace elements, as well as Sr–Nd–Os isotopic compositions for Yangyuan samples.

3. Analytical methods

Olivines from 80 Yangyuan peridotites were analyzed in mineral mounts using a JEOL 8900 Electron Probe Micro-analyzer (EPMA) at the University of Maryland (UMd) in order to obtain an overview of the compositional variation present within the suite. The EPMA analyses were performed using wavelength dispersive spectroscopy (WDS) with a 15 kV accelerating voltage, a 20 nA cup current, and a 10 μm diameter beam. A variety of natural materials were used as primary and secondary standards. Raw X-ray intensities were corrected using a ZAF algorithm. Twelve samples spanning the entire range of Fo (molar $Mg/(Mg + Fe^{2+}) \times 100$ of olivine) found in the suite, i.e., 90.2 to 92.0, were then selected on the basis of sample size and freshness for further study. These samples were pulverized following the procedures described in Rudnick et al. (2004) and polished thin sections were analyzed by EPMA for mineral compositions (Table S1) using the conditions cited above. Additional analyses of spinels from the Hannuoba peridotites were carried out at UMd in

order to compare with the earlier data of Rudnick et al. (2004) that were partially determined at Harvard University. The results are the same, within uncertainty.

Sulfides were examined using reflected light microscopy. Sulfides in several representative samples from Yangyuan and Hannuoba were selected for analysis by EPMA employing WDS techniques with the following operating conditions: an accelerating voltage of 15 kV, a cup current of 50 nA, and a fully focused 1 μm diameter beam. During the course of analyses, Si was monitored to assess beam overlap with silicate phases, and any analyses with detectable SiO_2 were discarded. X-ray counts were corrected using the ZAF method. A series of natural and pure element standards (e.g., pyrrhotite, chalcopyrite, olivine, Ni, and Cu) were used as both primary and secondary standards.

Major and minor elements in whole rock Yangyuan peridotites (see Table 1) were measured at Franklin and Marshall College using X-ray Fluorescence (XRF) techniques following the methodology of Boyd and Mertzman (1987). The accuracy of the measurements is typically ±1% for major elements having concentrations greater than 0.5%, and ±5% for the remaining elements.

In the analyses of HSE abundances and Os isotopes, sample powders were digested and equilibrated with isotope spike solutions by acids (a 2:1 mixture of distilled concentrated HNO_3 and HCl) in pre-cleaned (using aqua regia) sealed Pyrex Carius tubes for four days at 270 °C at UMd. HSE abundances and Os isotopes were determined through isotope dilution. The procedures have been detailed previously (e.g., Puchtel et al., 2009). Osmium was measured via negative thermal ionization mass-spectrometry (N-TIMS; *VG Sector 54* using electron multiplier) (Creaser et al., 1991; Volkening et al., 1991), while the remaining HSE were determined using an Aridus desolvating nebulizer coupled to a *Nu Plasma* MC-ICP-MS (using electron multipliers). Average blanks are: Os (0.38 ± 0.21), Ir (0.41 ± 0.33), Ru (2.0 ± 1.4), Pt (6.8 ± 2.3), Pd (10 ± 3) and Re (1.4 ± 0.5) pg (all uncertainties quoted are one sigma of 10 blank measurements). Blank corrections for Os, Ir, Ru, Pt and Pd are negligible (less than 0.2%) for most samples, except for the Pd blank in the Yangyuan samples, which constituted 0.5 to 6% of the total Pd. The Re blank makes up 0.3% to 17% of the total Re in all samples, where >2% uncertainties are noted in Table 2.

Because some studies have advocated higher pressure/temperature dissolutions than are commonly performed using Carius tubes in order to assure complete digestion of HSE-bearing phases, we also digested a subset of Hannuoba samples using an *Anton Paar* High Pressure Asher (HPA) for ~3 h at 280 °C and 130 b. Two Hannuoba samples measured by Becker et al. (2006) (DMP series) and re-analyzed here by HPA, yield Os isotopic compositions and HSE abundances within uncertainties of those previously reported. Five additional Hannuoba samples (DA20 series) from the study of Zhang et al. (2009) were measured by Carius tube digestion and three of these were also measured using HPA. Both methods produced results within uncertainties for a given sample. However, Os concentrations and isotopic compositions determined at UMd are substantially different from those reported in Zhang et al. (2009), which were analyzed by Os-sparging-MC-ICP-MS after NiS fusion. Likewise, four Yangyuan samples analyzed by sparging from the study of Y.G. Xu et al., (2008) studied here give significantly higher Os isotopic ratios than previously reported (Table 2). Further discussion of these results is provided in the electronic supplement (e.g., Table S2, Figs. S3 and S4).

Sulfur contents of Yangyuan samples were determined using high temperature combustion combined with infrared spectrometry at the Université du Québec à Chicoutimi, the protocol of which was described in Bédard et al. (2008). The S quantification limit for this method is ~22 ppm (Bédard et al., 2008). Selenium concentrations were also determined at the Université du Québec à Chicoutimi by instrumental neutron activation analysis (INAA) employing preconcentration of Se with thiol cotton fiber (TCF). The Se quantification limit is ~10 ppb for 1–3 g of material (Savard et al., 2006), the

Table 1
Whole rock analyses for Yangyuan peridotites (determined using XRF) and EPMA olivine forsterite (Fo) content (determined using EPMA).

Samples	YY-04	YY-08	YY-09	YY-11	YY-13	YY-22	YY-26	YY-27	YY-51	YY-52	YY-58	YY-60
SiO_2	43.88	44.38	44.44	42.45	43.76	43.96	43.39	42.77	41.34	43.67	43.75	42.52
TiO_2	0.04	0.08	0.09	0.05	0.11	0.05	0.08	0.12	0.03	0.08	0.07	0.05
Al_2O_3	1.63	2.97	3.04	1.77	2.44	2.45	3.08	2.87	1.12	2.70	2.40	1.26
Fe_2O_3T	8.00	8.79	8.39	9.22	8.70	8.25	8.76	9.49	8.54	8.52	8.07	8.86
MnO	0.13	0.14	0.14	0.14	0.13	0.13	0.14	0.15	0.13	0.14	0.13	0.13
MgO	44.39	39.90	40.77	44.79	41.87	42.26	41.65	41.16	46.02	41.50	42.37	44.85
CaO	1.03	2.89	2.12	1.08	1.90	1.81	2.15	2.48	1.40	2.26	2.00	1.23
Na_2O	0.02	0.11	0.13	0.03	0.11	0.08	0.10	0.13	0.02	0.12	0.12	0.03
K_2O	0.012	0.015	0.003	–	0.008	–	–	–	0.004	0.008	0.005	0.020
P_2O_5	0.01	0.02	0.02	0.02	0.02	0.02	0.02	0.02	0.02	0.02	0.02	0.02
Total	99.14	99.30	99.14	99.55	99.05	99.01	99.37	99.19	98.62	99.02	98.94	98.97
LOI	0.22	0.22	0.22	0.06	0.72	−0.06	0.06	0.26	−0.07	0.66	0.18	0.15	0.65
Cr	2485	2510	2520	1330	2280	2720	2850	2085	5480	2240	2610	2190
Ni	2730	2170	2670	3030	2870	2660	2830	2870	3660	2895	3100	3295
WR Mg#	91.7	90.0	90.6	90.6	90.5	91.0	90.4	89.6	91.4	90.6	91.2	90.9
Fo	92.0	90.5	90.9	90.8	90.9	91.2	90.7	90.2	91.6	90.8	91.7	91.3

Major oxides: wt.%; Fe_2O_3T: total Fe; Cr and Ni: ppm; LOI: loss on ignition; and WR Mg # and Fo: molar $Mg/(Mg+Fe^{2+}) \times 100$ in whole rock and olivine, respectively.

amounts used here. Details of the Se/TCF-INAA technique are outlined in Savard et al. (2006).

4. Results

Major and minor element compositions for Yangyuan peridotites are given in Table 1, along with Fo contents of olivines. Mineral compositions of the Yangyuan peridotites are provided in the electronic supplement. Forsterite contents of Hannuoba peridotites range from 89.5 to 91.6 (Rudnick et al., 2004), whereas Yangyuan peridotites range to slightly more refractory compositions (e.g., Fo = 90.2 to 92.0). These two suites of peridotites display many other compositional similarities including concentrations of MgO (36.7–43.9% vs. 39.9–46.1% for Hannuoba vs. Yangyuan, respectively), Al_2O_3 (1.2–3.9% vs. 0.9–3.1%), and CaO (1.0–3.5% vs. 0.5–2.9%) (Fig. 1). Thus, Hannuoba and Yangyuan peridotites are chemically similar with respect to major and minor element compositions.

Based on the empirical olivine–spinel oxygen barometer of Ballhaus et al. (1990), oxygen fugacities (fO_2) of the peridotites were calculated from the olivine and spinel compositions, assuming that spinels are perfectly stoichiometric ($MO:M_2O_3 = 1:1$). For this calculation, temperature was calculated from the orthopyroxene–clinopyroxene thermometer of Brey and Köhler (1990), assuming a pressure of 1.5 GPa. The resulting calculated fO_2 estimates are provided in Table 2. Yangyuan peridotites are generally characterized by a higher fO_2 (ΔFMQ: −0.7 to 0.2, with an average of −0.2) compared to Hannuoba peridotites (ΔFMQ: −3.6 to −0.4 with an average of −1.5) (Fig. 2).

Sulfide abundances are highly variable in Hannuoba peridotites, ranging from no observed sulfides (e.g., samples DMP-25 and DMP-67c) to hundreds of sulfides per thin section (e.g., DMP-60, Table 2). The abundances of sulfides are generally positively correlated with the sulfur contents of the whole rocks (Fig. S1). Both enclosed (Type-e) and interstitial (Type-i) base metal sulfides are present in Hannuoba peridotites (Fig. 3). Type-i sulfides are more abundant than Type-e sulfides (Fig. 4). The Hannuoba sulfides (<1 μm to 250 μm in diameter) range in shape from spherical, sub-spherical to polyhedral blebs (Fig. 3). Pentlandite is dominant relative to chalcopyrite (Fig. 4 and Table S3), and both may occur within the same sulfide (Fig. 3a and c). Considering their similar compositions, both Type-e and Type-i sulfides likely formed as immiscible melts trapped during partial melting (Szabo and Bodnar, 1995). At least some of these sulfides subsequently experienced exsolution and recrystallization, either in the mantle, or during entrainment in the host basalts (Szabo and Bodnar, 1995), resulting in formation of secondary sulfides, e.g., sulfide chains along healed fractures in silicates (Type-f) or veins along grain boundaries (Type-iv) (Fig. 3d

and e, respectively). Type-f and Type-iv secondary sulfides are indistinguishable mineralogically and chemically from the Type-e and Type-i sulfides (Fig. 4, Table S3). In addition to primary and high temperature secondary sulfides, Ni-rich sulfides (e.g., millerite, godlevskite, and heazlewoodite), are spatially associated with grain boundary serpentine, and may have formed as a result of serpentinization at low temperatures (Klein and Bach, 2009).

In comparison, despite similar or slightly lower fertility compared to Hannuoba peridotites, Yangyuan peridotites are sulfide-poor. Thin sections typically contain less than two sulfide grains, and most have none (Table 2). The sulfides are mostly rounded inclusions of mss, or multiphase assemblages of mss, pentlandite and/or chalcopyrite. Mss grains typically are metal-deficient, as evidenced by their low atomic (Fe + Ni + Cu)/S ratios (0.87 ± 0.04, 2σ), while both pentlandites and chalcopyrites from Yangyuan, as well as all Hannuoba sulfides are metal-saturated, given their near perfect stoichiometric metal-to-S ratios (Table S3).

Highly siderophile elements, Os isotopes, S, and Se data are provided in Table 2. In general, Hannuoba peridotites show a large range of S (20–320 ppm) (Gao et al., 2002) and Se (11–230 ppb) concentrations, broadly correlating with major element depletion indices, such as MgO and Al_2O_3 (e.g., Gao et al., 2002, and Fig. S1 in electronic supplement). The only exception to this is sample DMP 67c, which has a very low S content and sulfide abundances that are incongruous with its apparent fertility. Consistent with previous studies, Hannuoba peridotites display HSE patterns (normalized to CI chondrites) that are globally similar to those of primitive upper mantle (PUM; Becker et al., 2006), except for two samples—the refractory sample DMP 25, and the previously mentioned low-sulfur (and sulfide) sample DMP-67c (Fig. 5a). No obvious Os–Ir fractionation appears in the Hannuoba suite. Nevertheless, despite the generally PUM-like patterns, chondrite-normalized $(Pd/Ir)_N$ are well correlated with melt depletion indices, such as Al_2O_3 (Fig. 6), and overlap with ratios commonly observed in massif peridotites (e.g., Pearson et al., 2004; Becker et al., 2006; Luguet et al., 2007). Re/Os ratios are also similarly correlated with degree of melt extraction.

By contrast, despite spanning a range of melt depletion similar to that of the Hannuoba peridotites, the Yangyuan peridotites are characterized by much lower S (at or below the quantification limit of ~22 ppm) and Se contents (at or below the quantification limit of ~10 ppb, except for one sample having 43 ppb). Yangyuan peridotites also have significantly lower total HSE concentrations (ΣOs, Ir, Ru, Pt, Pd and Re) of 3 to 16 ppb, compared to Hannuoba peridotites, which have 17 to 32 ppb. Moreover, the HSE patterns of Yangyuan samples are characterized by striking Os, Pd and Re depletions, relative to Ir (Fig. 5b). Such fractionated patterns do not appear in the Hannuoba suite. Similar depletions in Os, Pd and Re,

Table 2
Highly siderophile elements, S and Se abundances, Os isotopic compositions, and fO_2 of Yangyuan and Hannuoba peridotites.

Sample	Os ppb	Ir ppb	Ru ppb	Pt ppb	Pd ppb	Re ppb	RBP[e] (%)	$^{187}Re/^{188}Os$	$^{187}Os/^{188}Os$	$(Pd/Ir)_N$[f]	Al_2O_3[g] (%)	Fo	S[h] ppm	Se ppb	fO_2[i] (ΔFMQ)	T_{RD}[j] Ga	T_{MA}[j] Ga	n[k]
Yangyuan locality																		
YY-04	1.27	2.50	4.79	2.76	0.89	–		–	0.11499	0.29	1.63	92.0	<22	–	− 0.7	1.8	-	n.f.
YY-04R	1.18	2.54	4.40	2.78	0.84	0.019	7	0.076	0.11516	0.27						1.8	2.1	
YY-08	0.847	2.39	4.59	3.20	1.62	0.023	4	0.13	0.12605	0.55	2.97	90.5	<22	43	0.0	0.15	0.21	2
YY-09	0.495	1.86	3.79	2.64	0.98	0.015	5	0.15	0.12163	0.43	3.04	90.9	<22	–	− 0.1	0.81	1.3	n.f.
YY-11	0.213	0.74	1.64	0.63	0.19	0.005	17	0.1	0.12116	0.21	1.77	90.8	<22	–	− 0.4	0.88	1.2	n.f.
YY-13	0.387	1.02	2.08	1.42	–	0.014	7	0.17	0.12102		2.44	90.9	<22	<10	0.1	0.90	1.5	n.f.
YY-13R	0.351	0.98	2.03	1.38	0.51	0.010	13	0.14	0.12117	0.42						0.88	1.3	
YY-22	0.925	2.98	4.81	5.07	1.83	0.045	2	0.23	0.12072	0.50	2.45	91.2	<22	–	− 0.5	0.99	2.3	n.f.
YY-22R	1.15	2.98	5.03	5.27	1.87	0.047	3	0.20	0.12063	0.51						0.98	1.88	
YY-26	1.07	2.64	4.41	2.94	0.60	0.103		0.462	0.11891	0.18	3.08	90.7	24	<10	− 0.5	1.2	-8.6	1
YY-26R	0.766	2.46	4.17	2.83	0.55	0.103		0.647	0.11966	0.18						1.1	-1.8	
YY-27	–	1.92	4.21	2.93	0.93	0.018	4	–	–	0.39	2.87	90.2	<22	–	− 0.1	–	–	n.f.
YY-27R	1.14	2.10	4.57	3.64	0.97	0.015	9	0.065	0.11948	0.37						1.1	1.3	
YY-51	2.34	2.93	6.18	2.47	0.39	0.009	11	0.02	0.11601	0.11	1.12	91.6	<22	–	0.2	1.6	1.7	n.f.
YY-51R	2.21	2.79	5.88	2.99	0.41	0.007	21	0.01	0.11639	0.12						1.6	1.6	
YY-52	0.520	1.32	2.89	2.24	0.76	0.022	5	0.20	0.12345	0.47	2.70	90.8	<22		0.2	0.54	1.1	n.f.
YY-58	0.511	1.82	3.32	2.96	1.09	0.024	4	0.23	0.12122	0.48	2.40	91.7	27	<10	− 0.1	0.87	2.0	2
YY-60	0.399	1.67	3.26	3.13	0.45	0.020	5	0.24	0.12079	0.22	1.26	91.3	<22	–	0.0	0.94	2.3	n.f.
YYB-2	1.28	1.85	3.56	3.33	0.75	0.020	4	0.076	0.11861	0.33	1.45	91.8	<22	–	–	1.3	1.5	
YYB-2R[a]	1.40								0.1124							2.1	-	
YYB-4	0.738	2.67	5.25	4.67	1.82	0.061	2	0.39	0.12016	0.55	2.15	91.9	–	–	–	1.0	40	
YYB-4R[a]	0.797								0.1146							1.8	–	
YYB-7	0.785	1.32	3.41	1.24	0.71	0.024	4	0.15	0.11525	0.43	0.89	91.8	–	–	–	1.7	2.7	
YYB-7R[a]	1.37								0.1110							2.3	–	
YG-18	1.78	2.83	5.01	2.68	0.72	0.017	5	0.046	0.11633	0.20	1.20	90.6	–	–	–	1.6	1.8	
YG-18R[a]	2.67								0.1106							2.4	–	
Hannuoba locality																		
DMP 04[b]	3.76	3.56	7.41	6.62	4.96	0.211		0.271	0.12289	1.13	2.29	91.1	73	40	− 0.7	0.63	1.9	64
DMP 19[b]	4.13	4.34	8.54	8.53	6.66	0.181		0.211	0.11998	1.24	1.91	91.3	91	28	− 1.0	1.1	2.2	50
DMP 19R	3.76	4.26	8.33	7.79	6.66	0.169		0.216	0.11996	1,27						1.0	2.2	
DMP 25	3.23	2.49	5.71	3.55	2.13	0.030	3	0.045	0.11660	0.69	1.61	91.6	20	11	− 0.4	1.5	1.7	n.f.
DMP25R[b]	2.70	2.27	5.14	3.46	–	0.032	3	0.056	0.11678							1.5	1.7	
DMP 41[b]	2.91	3.00	5.82	5.5	4.25	0.172		0.285	0.12327	1.15	2.76	90.4	110	–	− 3.6	0.57	1.9	
DMP 51	3.01	3.06	6.37	5.21	4.18	0.130		0.208	0.12309	1.10	1.96	91.1	130	31	− 1.3	0.59	1.2	135
DMP 56[b]	3.55	3.21	6.34	6.60	5.69	0.257		0.35	0.12748	1.43	3.49	89.9	260	46	− 1.3	− 0.1	− 0.6	
DMP 58[b]	3.78	3.59	7.33	6.96	5.86	0.190		0.242	0.12539	1.32	3.16	90.2	230	–	− 1.3	0.25	0.60	180
DMP 60[b]	4.00	3.59	7.24	7.31	6.21	0.303		0.365	0.12628	1.40	3.67	90.1	320	230	− 2.8	0.13	1.2	208
DMP 67c	1.66	1.27	1.58	3.00	1.74	0.036	4	0.10	0.12242	1.11	3.78	89.5	23	–	− 0.1	0.69	0.91	n.f.
DA20-02	3.63	3.41	7.06	7.18	6.24	0.333		0.443	0.12535	1.48	3.12	90.1	–	–	–	0.25	− 2.5	
DA20-02R[c]	3.64	3.54	7.05	7.10	5.90	0.349		0.461	0.12551	1.35						0.24	–	
DA20-02R[d]	6.18					0.295		0.229	0.11867							1.2	–	
DA20-05	3.45	3.59	7.42	7.44	5.55	0.240		0.336	0.12329	1,25	2.71	91.1	–	–	–	0.55	3.3	
DA20-05R[c]	3.23	3.67	7.47	7.25	5.35	0.231		0.344	0.12360	1.18						0.51	3.4	
DA20-05R[d]	5.76					0.241		0.201	0.11512							1.8	–	
DA20-16	3.60	2.62	6.41	5.52	4.91	0.054	2	0.073	0.12377	1.52	1.20	89.6	–	–	–	0.48	0.59	
DA20-16R[d]	3.79					0.077		0.098	0.12270							0.64	–	
DA20-17		3.83	7.76	6.90	5.74	0.094		0.14	0.12318	1.21	2.4	90.5	–	–	–	0.57	0.88	
DA20-17R[d]	4.95					0.082		0.079	0.11896							1.2	–	
DA20-19	2.44	2.79	6.04	5.37	4.71	0.137		0.271	0.12701	1.37	3.74	89.6	–	–	–	0	− 2.5	
DA20-19R[c]	2.39	2.94	6.02	6.32	4.43	0.139		0.279	0.12715	1.22						0	–	
DA20-19R[d]	5.08					0.012		0.011	0.11382							1.9		

Note: R represents an analytical replicate of the sample.

[a] Osmium data are from Y.G. Xu et al. (2008) by Os-sparging ICP-MS with four significant figures for $^{187}Os/^{188}Os$; all others with five significant figures.

[b] HSE data of Hannuoba peridotites are from Becker et al. (2006).

[c] Dissolution by HPA; all other samples in this study were dissolved by Carius tube digestion.

[d] Re–Os data are from Zhang et al. (2009) by Os-sparging ICP-MS.

[e] RBP depicts the Re blank percentage of the samples, where >2% is provided.

[f] Chondrite(Orgueil from Horan et al., 2003)-normalized Pd/Ir ratios.

[g] Al_2O_3 contents of DMP series of Hannuoba samples are from Gao et al. (2002). Those of DA20 series are from Zhang et al. (2009).

[h] S contents of Hannuoba peridotites are from Gao et al. (2002) with blanks of ~0.3 ppm.

[i] Oxygen fugacity (fO_2) is denoted by divergence from the fayalite–magnetite–quartz buffer (ΔFMQ). Mineral compositions of Hannuoba peridotites are from Rudnick et al. (2004).

[j] The parameters used in model age calculation are: $\lambda_{Re} = 1.666 \times 10^{-11}$/year ($^{187}Re/^{188}Os$)CI = 0.40186, ($^{187}Os/^{188}Os$)CI,0 = 0.1270 (Shirey and Walker, 1998).

[k] The number of sulfide grains per thintion. n.f. means 'not found'.

relative to Ir, have been observed in several other xenolithic peridotite suites worldwide, including Oak Creek, Sierra Nevada, USA (Lee, 2002), Cima, Basin and Range, USA (Lee, 2002), Vitim, Siberia (Pearson et al., 2004), North Queensland, Australia (Handler et al., 1999; Handler and Bennett, 1999), and Penglai, North China Craton (Chu et al., 2009) (Fig. S2 in the electronic supplement).

5. Discussion

Xenolithic peridotites entrained by basalts or kimberlites are fragments of the lithospheric mantle that formed as residues produced by partial melting of asthenospheric mantle. In addition to melt depletion, lithospheric peridotites may also record the effects of
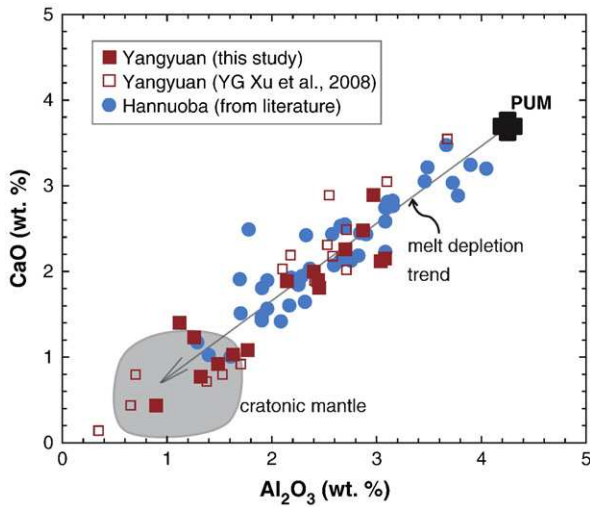
Fig. 1. Whole rock CaO versus Al_2O_3 (in wt.%) of Yangyuan and Hannuoba peridotites. Open squares of Yangyuan peridotites are from Y.G. Xu et al. (2008). Hannuoba data are from Song and Frey (1989), Chen et al. (2001), Rudnick et al. (2004), Choi et al. (2008), and Zhang et al. (2009). PM: primitive mantle (McDonough and Sun, 1995). Cratonic mantle data are from Boyd and Mertzman (1987), Boyd et al. (1993) and Pearson et al. (2004).

secondary processes. Here, we consider the effects of both partial melting and secondary processes on the relative and absolute abundances of the HSE in lithospheric peridotites underlying the North China Craton, and what effects these processes have had on model ages based on Os isotopes.

5.1. Partial melting

Partial melting of mantle peridotite is an important process leading to the formation of lithospheric mantle. Given the typical established relative order of the compatibility of HSE (Os ~ Ir ~ Ru > Pt > Pd > Re) (Pearson et al., 2004), melt extraction progressively results in depletions of PPGE and Re relative to the more refractory IPGE (Bockrath et al., 2004; Pearson et al., 2004; Ballhaus et al., 2006). Thus, $(Pd/Ir)_N$, combined with an indicator of melt depletion, such as whole rock Al_2O_3, can potentially be used to assess whether HSE fractionations were caused by primary melting or secondary processes.
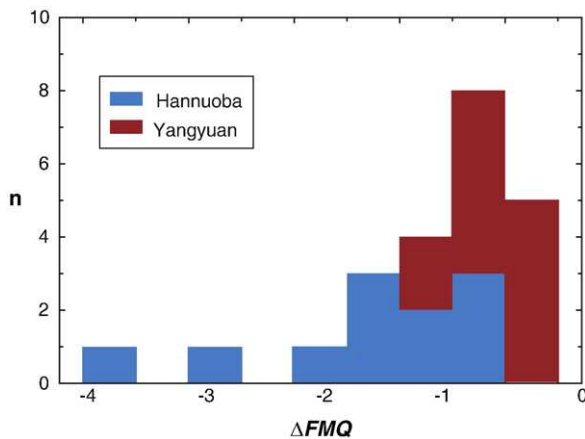
Fig. 2. Oxygen fugacities (fO_2) of Yangyuan and Hannuoba peridotites calculated based on the empirical olivine–spinel barometer (assuming P = 1.5 GPa) of Ballhaus et al. (1990). Mineral compositions of Hannuoba peridotites are from Rudnick et al. (2004). Spinel analyses from this previous study, which were partially determined at a different laboratory, were verified to be consistent with data from this study.

The $(Pd/Ir)_N$ of Hannuoba peridotites, except for samples DMP-67c and DA20-16, are positively correlated with Al_2O_3, and overlap with the range defined by orogenic massif peridotites (model lower curve in Fig. 6). Hannuoba samples also display a rough negative correlation between MgO and S (Gao et al., 2002; except for S-poor sample DMP-67c) or Se (see electronic supplement; except for sample DMP-60 with an extremely high Se content of 230 ppb), which is consistent with these samples having formed as residues of varying extents of partial melting, with subsequent preservation of sulfides. Moreover, the sulfides in the Hannuoba peridotites are indistinguishable mineralogically and chemically, irrespective of their position (grain boundary, inclusion, and healed fracture) or morphology, and are dominated by pentlandite; chalcopyrite is rare and generally forms as exsolution rims on pentlandite (Figs. 3 and 4). This observation suggests little addition of secondary, Cu-rich sulfides (cf. Alard et al., 2000; X.S. Xu et al., 2008). In addition, Hannuoba peridotites exhibit a whole rock Re–Os errorchron and a positive correlation between $^{187}Os/^{188}Os$ and Al_2O_3 (excluding samples DMP-67c and DA20-16) (Fig. 7), which also likely reflects the dominant effects of partial melting (Gao et al., 2002). Alternatively, Zhang et al. (2009) proposed that Hannuoba peridotites are Archean residues that experienced late melt refertilization. However, addition of basaltic or picritic melts, which have high Al_2O_3 and low Os contents relative to ancient residual peridotite, would have little impact on Os isotopic compositions, but a much greater impact on the Al_2O_3 contents of the peridotites (Fig. 7). Such refertilization will result in strongly curved mixing arrays on Al_2O_3 vs. $^{187}Os/^{188}Os$ plots (Reisberg and Lorand, 1995), which are not observed in the Hannuoba data (Fig. 7). We conclude that most Hannuoba samples are unlikely to have experienced melt refertilization long after melt depletion. Thus, the compositional and petrographic features highlighted above, as well as the similarities to massif peridotites, indicate that partial melting was the dominant process affecting HSE and Os isotopes in Hannuoba samples.

In contrast to the Hannuoba samples, $(Pd/Ir)_N$ of Yangyuan peridotites show no clear correlation when plotted against Al_2O_3, and most samples plot below the trend defined by the Hannuoba and massif peridotite data (Fig. 6). The inter-element HSE fractionations of Yangyuan peridotites cannot simply be the result of a single stage of partial melting, because partial melting alone would not fractionate Os from Ir and Ru, given similar geochemical compatibilities of IPGE. Further, the peridotite's Pd/Ir and Re/Ir ratios are much lower than would be consistent with their fertility (e.g., Fig. 6). Thus, the distinct HSE characteristics of Yangyuan samples must reflect secondary processes, rather than primary melt depletion. Similar HSE characteristics have been observed in other alkali-basalt-hosted peridotite xenoliths worldwide (e.g., Handler et al., 1999; Lee, 2002; Pearson et al., 2004; Chu et al., 2009), suggesting that certain recurring secondary processes affect HSE abundances of xenolithic peridotites in a systematic manner.

5.2. Secondary processes

Secondary processes that may affect whole rock HSE abundances include serpentinization, refertilization via melt addition (Saal et al., 2001), mantle metasomatism via melt–rock reaction (Büchl et al., 2002), and sulfide breakdown prior to, during, or subsequent to entrainment and eruption of the host basalt (Handler et al., 1999; Handler and Bennett, 1999; Lorand et al., 2003a; Reisberg et al., 2005). The latter may occur via several processes, which are discussed below.

5.2.1. Serpentinization

The Yangyuan samples are devoid of serpentine, so serpentinization cannot explain their fractionated HSE patterns. Furthermore, although we observe minor serpentinization along grain boundaries of some Hannuoba peridotites (e.g., DMP-19), there is no correlation
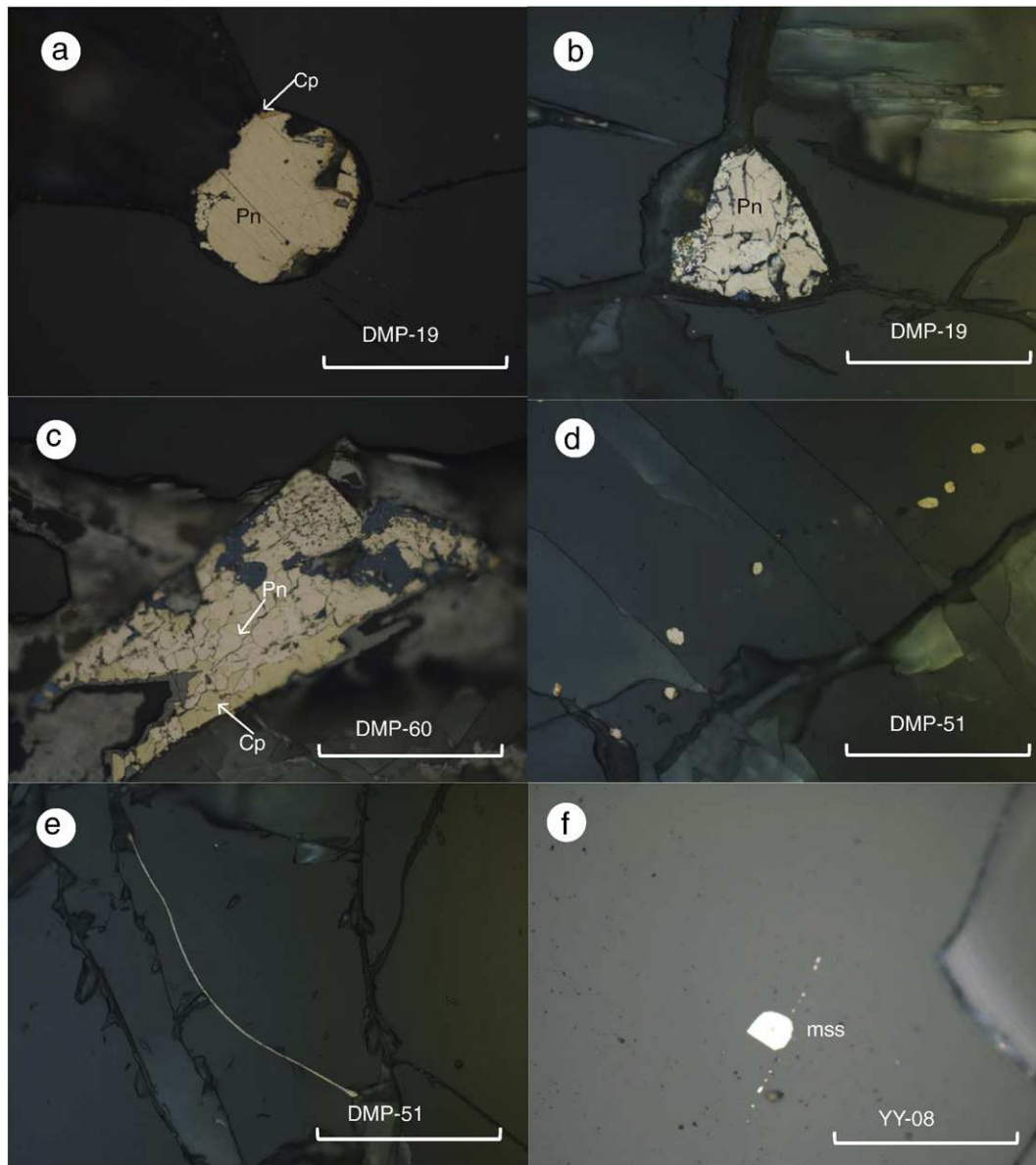
Fig. 3. Photomicrographs of sulfides in the Hannuoba and Yangyuan peridotites under reflected light microscopy (scale bar equals 100 μm). Hannuoba: a. Type-e sulfide occurs as an inclusion in olivine; b. Type-i sulfide occurs at the triple junction of silicates; c. Type-i sulfides with a polyhedral texture; d. Type-f sulfides along healed fractures; and e. Type-iv sulfides along grain boundary. Yangyuan: f. Type-e mss as inclusion in olivine. Pn: pentlandite; Cp: chalcopyrite; and mss: monosulfide solid solution.

between the degree of serpentinization and HSE patterns, which are all rather uniform (Fig. 5). These observations are consistent with published data that suggests that the HSE remain stable during serpentinization, which occurs at relatively low temperatures in a reducing environment (Snow and Schmidt, 1998; Liu et al., 2009), in which sulfides are preserved (Klein and Bach, 2009).

5.2.2. Refertilization

Addition of melt to refractory peridotites (refertilization) will lead to enrichment of incompatible major and trace elements. For example, refertilization via basalt infiltration long after melt depletion will lead to Al_2O_3 enrichment, without significantly changing $^{187}Os/^{188}Os$, due to the very low abundances of Os in typical basalts (e.g., Reisberg and Lorand, 1995). Because mantle-derived melts are commonly enriched in Re and PPGE, relative to IPGE (e.g., Puchtel and Humayun, 2000), refertilization is normally expected to increase Pt, Pd and Re relative to Ir (e.g., Rehkämper et al., 1999; Lorand et al., 2009). This is the opposite of what is observed in the Yangyuan suite, and we conclude that refertilization is not responsible for the

distinctive HSE patterns of these samples. Nevertheless, several Yangyuan samples (i.e., YY-04, YY-09, YY-26, and YY-27) plot to the right of the trend defined by $^{187}Os/^{188}Os$ and Al_2O_3 (Fig. 7). These samples exhibit higher Al_2O_3 than others that have similar $^{187}Os/^{188}Os$, which can be explained by small degrees (<3%) of basalt addition long after melt depletion (Fig. 7). Given the similarity of the HSE patterns in all of these rocks, either this small amount of basalt addition did not influence the HSE patterns, or the process(es) responsible for the distinctive HSE patterns in the Yangyuan samples obliterated any fractionation associated with basalt addition.

5.2.3. Metasomatism via Melt–rock reaction

The effects of melt/fluid–rock reactions are frequently observed in mantle peridotites. For example, the enrichment of light rare earth elements (LREE) in refractory peridotites is commonly interpreted to result from mantle metasomatism (e.g., Frey and Green, 1974). This category of process is distinct from refertilization in that refertilization can add major phases to the affected lithology, while metasomatism may not affect the major mineralogy. In peridotites,
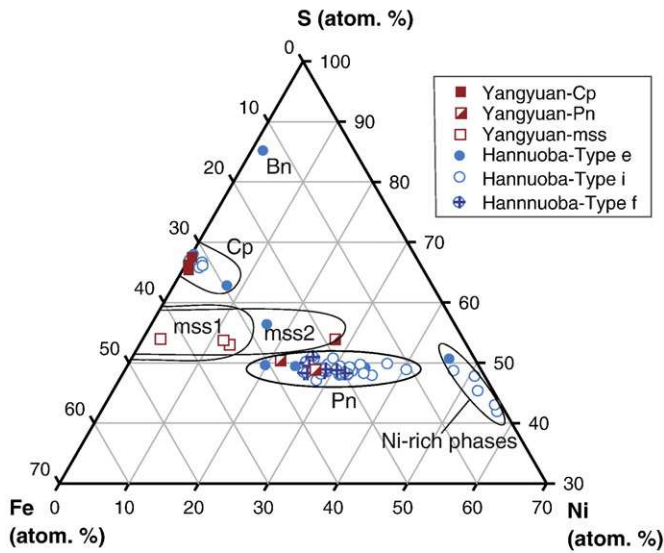
Fig. 4. Sulfide compositions plotted in the Fe–Ni–S system (Cu is subtracted and Fe, Ni and S are normalized to 100% atomic). All observed sulfides in Yangyuan peridotites are enclosed sulfides having mss, pentlandite (Pn) and/or chalcopyrite (Cp) compositions. Hannuoba sulfides are dominated by Pn with minor Cp and mss as well as Ni-rich phases (e.g., millerite (Ml), godlevskite (Gv), and heazlewoodite (Hw)). Bn: bornite. Phase fields mss1 and 2: 1100 °C and 1000 °C, respectively, according to Kullerud et al. (1969). Type-e: enclosed sulfides; Type-i: interstitial sulfides including sulfide veins along grain boundaries; and type-f: sulfide chains along healed fractures.

metasomatism can potentially result in sulfide precipitation (e.g., Alard et al., 2000; Luguet et al., 2003), or sulfide dissolution or breakdown (Büchl et al., 2002; Reisberg et al., 2005; Ackerman et al., 2009).

Trace element data, including LREE enrichment in some samples, suggest that melt/fluid–rock reaction occurred in some Yangyuan
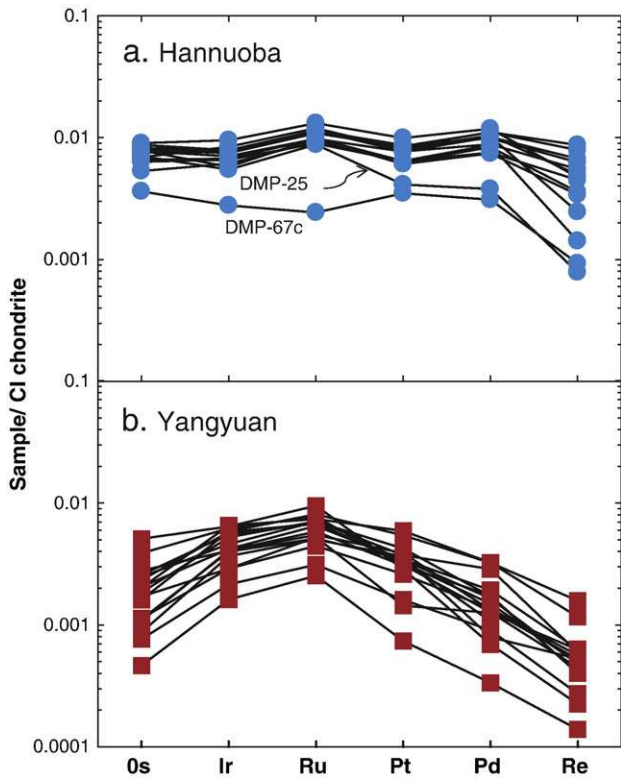

Fig. 5. HSE patterns of whole rock peridotites normalized to the CI chondrite, Orgueil (Horan et al., 2003): a. Hannuoba. b. Yangyuan. Some of the Hannuoba data are from Becker et al. (2006).
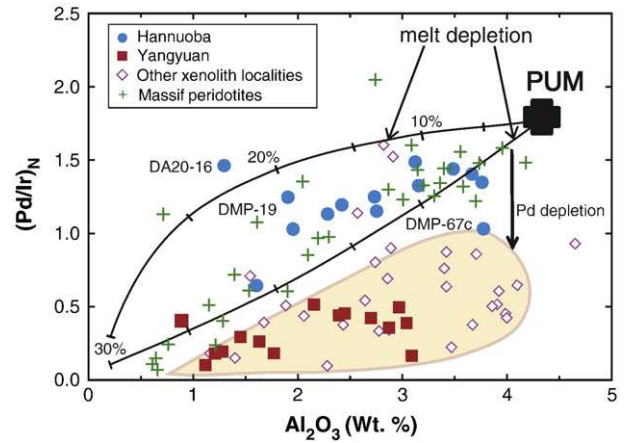
Fig. 6. Al_2O_3 versus $(Pd/Ir)_N$ for xenolithic peridotites from the North China Craton compared to other xenolithic and massif peridotites. Open diamond symbols depict xenoliths that show Os depletion relative to Ir from Vitim, Siberia (Pearson et al., 2004), North Queensland, Australia (Handler et al., 1999; Handler and Bennett, 1999), and Penglai, North China Craton (Chu et al., 2009). Melting model curves were calculated for non-modal, fractional melting using a primitive upper mantle (PUM) source containing 300 ppm S, while the extracted melts have a S capacity of 1000 ppm. The partition coefficients between sulfide and melt, $D_{HSE(sulfide/melt)}$, used in the models are: $D_{Pd(sulfide/melt)}$ of 10^4 and 10^3 for model upper curve and lower curve, respectively, according to Fleet et al (1999); $D_{Ir(sulfide/melt)}$ was set at 10^5. Tick marks show 5% melting increments. Data sources: PUM is from Becker et al. (2006) and McDonough and Sun (1995). Massif data are from a variety of literature sources for the following locations: Pyrenees (France) (Becker et al., 2006; Luguet et al., 2007; Lorand et al., 2008b), Italian Alps (Becker et al., 2006), Beni Bousera (Morocco) (Pearson et al., 2004), Ronda (Spain) (Becker et al., 2006), Lower Austria (Becker et al., 2006), and Ashaway (America) (Becker et al., 2006).

peridotites (Y.G. Xu et al., 2008). For example, sample YY-60 has an Os isotopic composition (0.1208) that is more radiogenic than would be consistent with its refractory composition (e.g., Al_2O_3: 1.26%, CaO: 1.23%, and Fo: 91.3). This Os isotopic composition may reflect addition of radiogenic sulfide prior to sulfide breakdown. Nevertheless, there is no evidence for substantial sulfide addition via metasomatism for the Yangyuan peridotites, which instead show a notable deficit of sulfides,
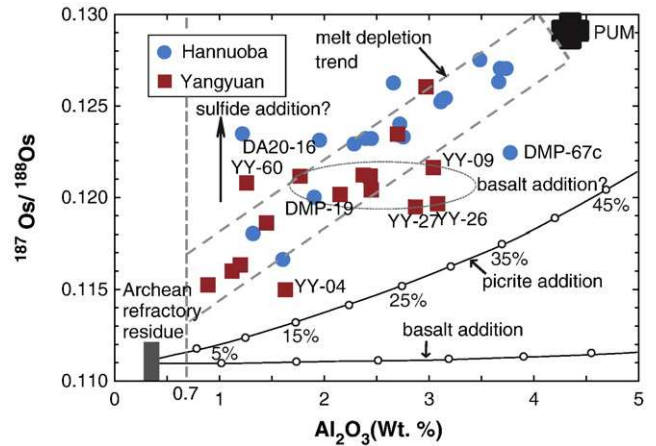
Fig. 7. Whole rock Al_2O_3 versus $^{187}Os/^{188}Os$ of Hannuoba and Yangyuan peridotites. A melt depletion trend is outlined by the dashed bar. PUM: Meisel et al., 2001 (for $^{187}Os/^{188}Os$) and McDonough and Sun, 1995 (for Al_2O_3). Hannuoba data sources: Meisel et al., 2001; Gao et al., 2002; Becker et al., 2006; and this study. Gray bar (labeled "Archean refractory residue") represents a refractory peridotite formed by high degrees of melt extraction at 2.2 to 2.5 Ga with $^{187}Os/^{188}Os$ ranging from 0.110 to 0.112, where all Re was lost during melting. Present-day refertilization of this residue by addition of picritic or basaltic melt is illustrated. Mixing parameters used: picritic melt has 1 ppb Os, 10 wt.% Al_2O_3 and an $^{187}Os/^{188}Os$ of 0.16; basaltic melt has 0.05 ppb Os, 15 wt.% Al_2O_3 and an $^{187}Os/^{188}Os$ of 0.16; the refractory peridotitic residue has 3.5 ppb Os, 0.3 wt.% Al_2O_3 and an $^{187}Os/^{188}Os$ of 0.111 ± 0.001. Open circles along curves represent increments of 5% melt addition. The vertical dashed line represents peridotites with Al_2O_3 of 0.7%, where peridotites lose all Re (Handler et al., 1997).

and have very low S and Se abundances that are consistent with the rarity of sulfides in the rocks. Furthermore, the addition of sulfides normally rich in PPGE and Re would tend to elevate PPGE/IPGE ratios (Rehkämper et al., 1999; Alard et al., 2000; Lorand et al., 2009), which is not observed. However, sulfide breakdown via melt–rock reaction under oxidizing conditions (e.g., Reisberg et al., 2005) may be responsible for the HSE patterns of the Yangyuan peridotites, as discussed in the next section.

5.2.4. Sulfide loss

Compared to Hannuoba and massif peridotites, the low whole rock S contents and the rarity of sulfides in the Yangyuan peridotites allow us to conclude that sulfide dissolution, removal and/or breakdown was likely a prime factor leading to their distinctive HSE patterns. Sulfur and sulfides could have been removed from these rocks by at least three processes.

One form of sulfur loss is through surficial weathering that may take place following eruption. This occurs when sulfides become oxidized and are then replaced by hydroxides and oxides, leading to S loss (Lorand, 1990). The ratio of S to a less mobile element that is enriched in sulfides, such as Cu (Handler et al., 1999) or Se (Lorand et al., 2003a), can be used to estimate the amount of oxidative sulfide breakdown that a peridotite xenolith has experienced. Selenium contents were determined for four relatively fertile Yangyuan peridotites, which would be expected to contain the greatest amount of original sulfides. Only one of these samples has Se above the quantification limit of ~10 ppb. Thus, the coupled low S and Se contents of most Yangyuan samples suggest that sulfide weathering was likely not the primary process that removed sulfides (e.g., Lorand et al., 2003a), and hence, was likely not the dominant process affecting their HSE. This conclusion is also consistent with the lack of secondary oxides or hydroxides in these samples, as well as the general immobility of HSE in peridotites that experience low temperature alteration (Rehkämper et al., 1999; Liu et al., 2009).

Lorand et al. (2003a,b) suggested an alternative means by which sulfides may be removed from peridotites. Sulfides, which are molten at mantle temperatures and have much higher densities than silicates, may drain downward in peridotite with high porosities (Lorand et al., 2003a,b). Such migration could result in low S and HSE contents (Lorand et al., 2003a,b). However, sulfide draining cannot account for at least some of the observed HSE fractionations in the Yangyuan peridotites, for example, Os depletion relative to Ir. Thus, this process is unlikely to have strongly impacted the Yangyuan HSE patterns.

Sulfide dissolution or breakdown during melt/fluid percolation or transit to the surface (e.g., Handler et al., 1999; Büchl et al., 2002; Lorand et al., 2003a; Reisberg et al., 2005) was most likely the process leading to the HSE characteristics of Yangyuan samples. Sulfide breakdown can strongly affect whole rock HSE concentrations. There are several processes that must be considered.

First, it has been suggested that melt–rock reaction at the high melt/rock ratios that produce replacive dunites, may destroy the majority of sulfides, stripping the peridotite of most HSE (Büchl et al., 2002). In this case, subsequent precipitation of sulfides from later melts will dominate the shape of HSE patterns as well as Os isotope composition in the replacive dunites, which may lead to low Os/Ir ratios, high Pd/Ir ratios, and melt-dominant radiogenic Os isotopic compositions (Büchl et al., 2002, 2004). However, there is no evidence for extensive melt–rock reaction in the Yangyuan suite; for example, there are no replacive dunites or evidence of secondary sulfide precipitation. Further, Yangyuan peridotites show very low Pd/Ir ratios and subchondritic $^{187}Os/^{188}Os$, rather than the suprachondritic Pd/Ir ratios and radiogenic $^{187}Os/^{188}Os$ seen in replacive dunites (Büchl et al., 2002). Thus, melt–rock reaction at a high melt/rock ratio is inconsistent with the observed HSE characteristics of Yangyuan peridotites.

Second, as Yangyuan peridotites exhibit somewhat higher fO_2 than those of Hannuoba peridotites, we consider the possibility of oxidative sulfide breakdown. During this process, S can be oxidized into more mobile sulfates and then lost from the rocks. When sulfide breaks down, the sulfide-borne HSE are released. They may either remain in the rocks as alloy phases, or be lost as volatiles, depending on their volatilities. Experimental data and thermodynamic calculations suggest that Pd metal and certain oxides of Os and Ru are volatile under highly oxidized conditions at high temperatures (greater than 1100 °C) (Wood, 1987). If the Yangyuan peridotites were highly oxidized, it might be expected that not only Pd and Os depletions would be present relative to Ir, but that Ru/Ir ratios would also be low. However, both Yangyuan and Hannuoba peridotites have essentially PUM-like $(Ru/Ir)_N$ ratios (1.40 ± 0.33 for Yangyuan and 1.46 ± 0.20 for Hannuoba, cf. 1.49 ± 0.18 for PUM, Becker et al., 2006). Furthermore, the calculated fO_2's of Yangyuan peridotites (Table 2) are much lower than those required to oxidize sulfides, i.e., $fO_2 = FMQ + 2$ or greater (Mungall et al., 2006). Finally, heating experiments have shown that Os volatilization loss is unlikely under mantle conditions (Wulf et al., 1995). Therefore, we conclude that oxidative sulfide breakdown was probably not responsible for producing the distinctive HSE patterns in the Yangyuan peridotites.

Lithophile trace element data document interaction between an invasive melt or fluid phase and the Yangyuan peridotites (Y.G. Xu et al., 2008). We propose that, in the presence of variable fO_2 and fS_2 conditions during melt–rock interaction, partition coefficients for HSE might change (Brenan, 2008; Fonseca et al., 2008). When melts/fluids are S-undersaturated, i.e., with a low fS_2, desulfurization, a process of S loss, may occur in the peridotites. In this process, sulfides may incongruently break down to form refractory mss, Pd-rich sulfide liquid, and Ir–Pt alloys (Peregoedova et al., 2004, 2006). Moreover, interaction with oxidized melts would impart a metal deficiency to any surviving mss (Eggler and Lorand, 1993), consistent with the mss compositions in the Yangyuan peridotites. Although metal-deficient mss is expected to have high partition coefficients for Os and Pd (Barnes et al., 2001), the lack of Os and Pd enrichments in the whole rocks, indeed, the observed depletion of these elements, means that the residual mss has had little leverage on the whole rock HSE content. Incongruent sulfide breakdown lowers total HSE abundances (Lorand et al., 2003a) and causes further fractionations of HSE (Handler et al., 1999), such as Pd depletions relative to Ir. Although the behavior of Os during incongruent sulfide breakdown has not yet been experimentally constrained (e.g., Peregoedova et al., 2004, 2006; Mungall et al., 2006), we propose that, in an oxidizing environment, it is possible to fractionate Os from Ir–Ru–Pt via this process. In such an environment, Os contained in HSE-hosting phases may be partially dissolved into the melt/fluid phase, leaving Ir–Ru–Pt to be taken up into refractory sulfides or alloys (Li et al., 1996; Barnes et al., 2001), creating the observed low Os/Ir ratios. In addition, Re becomes less chalcophile at higher fO_2 (Fonseca et al., 2008), which could explain the incompatible behavior of Re as well as low Re/Ir ratios in the Yangyuan peridotites.

5.3. Comparison of secondary processes in Yangyuan and Hannuoba peridotites

Compared to the Yangyuan peridotites, the S and Se concentrations and HSE patterns of Hannuoba peridotites do not show evidence for sulfide removal, except for sample DMP-67c, which is depleted in S and falls off the Re–Os correlation (Gao et al., 2002). This sample has low total HSE (Table 2, Fig. 5) and Pd/Ir ratio, but does not exhibit the low Os/Ir that is characteristic of the sulfide-depleted Yangyuan samples. These features suggest that the mechanism of sulfide depletion in this sample was different than that experienced by the Yangyuan samples.

Like the Yangyuan samples, Hannuoba peridotites also show evidence for melt/fluid metasomatism, based on lithophile trace element patterns (Song and Frey, 1989; Rudnick et al., 2004; Choi et al., 2008). However, there are no robust correlations between HSE and lithophile trace element patterns such as Pd/Ir vs. La/Yb, suggesting that HSE were less mobile than lithophile trace elements during this metasomatism. The lower fO_2 of the Hannuoba peridotites (Fig. 2) suggests that the metasomatic agent had a lower fO_2 and relatively high fS_2 compared to that at Yangyuan. Consequently, sulfides survived during melt/fluid–rock reaction, consistent with the presence of metal-saturated sulfides in this suite. Further, some sulfide precipitation may have occurred (X.S. Xu et al., 2008), as suggested by the extraordinarily high S and Se content of at least one Hannuoba peridotite (DMP-60, having 320 ppm S and 230 ppb Se), which has a higher proportion of Cu-rich sulfides than the other Hannuoba samples (Table S3). As this sample has the same general HSE pattern as the other Hannuoba peridotites (Fig. 5a), apparently sulfide addition did not heavily modify the HSE patterns, probably due to the relatively low HSE concentrations of these additional sulfides (Alard et al., 2000).

One Hannuoba sample, DA20-16, plots significantly to the left of the Al_2O_3 vs. $(Pd/Ir)_N$ and Al_2O_3 vs. $^{187}Os/^{188}Os$ trends (Figs. 6 and 7). This sample has a peculiar major element composition, with low whole rock Mg# (89.6) coupled with low Al_2O_3 and CaO (Zhang et al., 2009), suggesting that it experienced Fe enrichment without affecting the other major elements. Given the position of this sample on the HSE plots, it appears that the Fe enrichment likely accompanied sulfide addition, which could explain the elevated its Pd/Ir and $^{187}Os/^{188}Os$ ratios (Figs. 6 and 7).

5.4. Impact on Os isotopes

The effects of sulfide breakdown on Os isotopes appear to be minimal. If the suite of Yangyuan peridotites shared the same initial $^{187}Os/^{188}Os$, then the present-day $^{187}Os/^{188}Os$ of each sample should positively correlate with its $^{187}Re/^{188}Os$, assuming a closed system (i.e., the isochron principle). Over time, $^{187}Os/^{188}Os$ will reflect melt depletion, similar to Al_2O_3, given the moderate incompatibility of Re and the strong compatibility of Os during partial melting. As such, the present-day $^{187}Os/^{188}Os$ is related to fertility, i.e., the lower the $^{187}Os/^{188}Os$, the more refractory the rock is.

Although the Yangyuan peridotites appear to have lost sulfides, as documented above, the suite nevertheless shows a positive correlation between $^{187}Os/^{188}Os$ and robust immobile element indicators of melt depletion, such as olivine forsterite content, whole rock Yb, and Al_2O_3 (Fig. 7). Similar correlations are seen in samples from other suites that are characterized by fractionated Os/Ir (e.g., Pearson et al., 2004). Thus, incongruent sulfide breakdown does not appear to have affected Os isotopic compositions and, hence, Re depletion model ages (T_{RD}-minimum estimated age of melt depletion assuming no Re in the residue since formation, Walker et al., 1989). This suggests that the sulfide breakdown (and Re/Os fractionation) occurred relatively recently (i.e., since the Mesozoic). In contrast, Os model ages calculated using observed Re/Os relative to a chondritic reservoir (T_{MA}; Walker et al., 1989; Shirey and Walker, 1998) might dramatically change due to Re/Os fractionation.

Similar ranges of $^{187}Os/^{188}Os$ for Hannuoba and Yangyuan peridotites (0.116–0.127 vs. 0.115–0.126, respectively, Table 2) and their resulting similar T_{RD} model ages (Table 2), suggest that the Os model ages from our new data are robust. Omitting the outliers associated with refertilization and sulfide addition discussed above, the positive and overlapping $^{187}Os/^{188}Os$ vs. Al_2O_3 correlations for both Hannuoba and Yangyuan suites intersect 0.7 wt.% Al_2O_3 (the value considered best representative of maximum melt depletion in off-craton peridotites by Handler et al.(1997)) at $^{187}Os/^{188}Os$ of ~0.113 to 0.117, corresponding to model ages of ~1.6 to 2.0 Ga

(Fig. 7). By contrast, an Archean peridotite that has been refertilized by basaltic or picritic melts (e.g., Y.G. Xu et al., 2008; Zhang et al., 2009) would plot along the mixing lines depicted in Fig. 7—far from where any of the data plot. Thus, it is highly unlikely that the lithospheric mantle in this portion of the Trans-North-China Orogen formed in the Archean.

6. Conclusions

Variable but relatively low degrees of partial melting of the mantle can produce the HSE patterns observed in the Hannuoba peridotites, given long-term preservation of sulfides. By contrast, the distinct HSE patterns of Yangyuan peridotites, characterized by low total HSE and Os, Pd and Re depletions relative to Ir, cannot be produced by partial melting alone. These characteristics reflect secondary processes. Given the low S and Se of these samples and the metal-deficient composition of their mss, we suggest that incongruent sulfide breakdown occurred during interaction with a S-undersaturated melt/fluid under a high fO_2 and low fS_2. This resulted in S, Se, Os, Pd and Re loss relative to Ir and, thus, was likely an important process leading to the observed HSE characteristics in Yangyuan peridotites. The similarity of the Yangyuan HSE patterns to those of xenolithic peridotites from a number of other localities, worldwide, suggests that this process is common within some regions of the upper mantle.

Preservation of the correlation between $^{187}Os/^{188}Os$ and immobile melt depletion indices (e.g., Yb and Al_2O_3) indicates that incongruent sulfide breakdown was a recent event. The similarity of T_{RD} model ages of Yangyuan and Hannuoba peridotites is also consistent with this; both peridotite suites appear to have formed in the Paleoproterozoic (ca. 1.6–2.0 Ga).

Appendix A. Supplementary data

Supplementary data associated with this article can be found, in the online version, at doi:10.1016/j.epsl.2010.06.030.

References

Ackerman, L., Walker, R.J., Puchtel, I.S., Pitcher, L., Jelinek, E., Strnad, L., 2009. Effects of melt percolation on highly siderophile elements and Os isotopes in subcontinental lithospheric mantle: a study of the upper mantle profile beneath Central Europe. Geochim. Cosmochim. Acta 73, 2400–2414.

Alard, O., Griffin, W.L., Lorand, J.P., Jackson, S.E., O'Reilly, S.Y., 2000. Non-chondritic distribution of the highly siderophile elements in mantle sulphides. Nature 407, 891–894.

Ballhaus, C., Berry, R.F., Green, D.H., 1990. Oxygen fugacity controls in the Earth's upper mantle. Nature 348, 437–440.

Ballhaus, C., Bockrath, C., Wohlgemuth-Ueberwasser, C., Laurenz, V., Berndt, J., 2006. Fractionation of the noble metals by physical processes. Contrib. Mineralog. Petrol. 152, 667–684.

Barnes, S.-J., van Achterbergh, E., Makovicky, E., Li, C., 2001. Proton microprobe results for the partitioning of platinum-group elements between monosulphide solid solution and sulphide liquid. S. Afr. J. Geol. 104, 275–286.

Becker, H., Horan, M.F., Walker, R.J., Gao, S., Lorand, J.P., Rudnick, R.L., 2006. Highly siderophile element composition of the Earth's primitive upper mantle: Constraints

from new data on peridotite massifs and xenoliths. Geochim. Cosmochim. Acta 70, 4528–4550.

Bédard, L.P., Savard, D., Barnes, S.J., 2008. Total sulfur concentration in geological reference materials by elemental infrared analyser. Geostand. Geoanal. Res. 32, 203–208.

Bockrath, C., Ballhaus, C., Holzheid, A., 2004. Fractionation of the platinum-group elements during mantle melting. Science 305, 1951–1953.

Boyd, F.R., Mertzman, S.A., 1987. Composition of structure of the Kaapvaal lithosphere, southern Africa. In: Mysen, B.O. (Ed.), Magmatic Processes—Physicochemical Principles: The Geochemical Society, Special Publication, #1, pp. 13–24.

Boyd, F.R., Pearson, D.G., Nixon, P.H., Mertzman, S.A., 1993. Low-calcium garnet harzburgites from Southern Africa—their relations to craton structure and diamond crystallization. Contrib. Mineralog. Petrol. 113, 352–366.

Brenan, J.M., 2008. Re–Os fractionation by sulfide melt-silicate melt partitioning: a new spin. Chem. Geol. 248, 140–165.

Brey, G.P., Köhler, T., 1990. Geothermobarometry in four-phase lherzolites II. New thermobarometers, and practical assessment of existing thermobarometers. J. Petrol. 31, 1353–1378.

Büchl, A., Brugmann, G., Batanova, V.G., Munker, C., Hofmann, A.W., 2002. Melt percolation monitored by Os isotopes and HSE abundances: a case study from the mantle section of the Troodos Ophiolite. Earth Planet. Sci. Lett. 204, 385–402.

Büchl, A., Brugmann, G.E., Batanova, V.G., Hofmann, A.W., 2004. Os mobilization during melt percolation: the evolution of Os isotope heterogeneities in the mantle sequence of the Troodos ophiolite, Cyprus. Geochim. Cosmochim. Acta 68, 3397–3408.

Chen, S.H., O'Reilly, S.Y., Zhou, X.H., Griffin, W.L., Zhang, G.H., Sun, M., Feng, J.L., Zhang, M., 2001. Thermal and petrological structure of the lithosphere beneath Hannuoba, Sino-Korean Craton, China: evidence from xenoliths. Lithos 56, 267–301.

Choi, S.H., Mukasa, S.B., Zhou, X.H., Xian, X.H., Andronikov, A.V., 2008. Mantle dynamics beneath East Asia constrained by Sr, Nd, Pb and Hf isotopic systematics of ultramafic xenoliths and their host basalts from Hannuoba, North China. Chem. Geol. 248, 40–61.

Chu, Z.Y., Wu, F.Y., Walker, R.J., Rudnick, R.L., Pitcher, L., Puchtel, I.S., Yang, Y.H., Wilde, S.A., 2009. Temporal evolution of the lithospheric mantle beneath the eastern North China Craton. J. Petrol. 50, 1857–1898.

Creaser, R.A., Papanastassiou, D.A., Wasserburg, G.J., 1991. Negative thermal ion mass-spectrometry of osmium, rhenium, and iridium. Geochim. Cosmochim. Acta 55, 397–401.

Eggler, D.H., Lorand, J.P., 1993. Mantle sulfide geobarometry. Geochim. Cosmochim. Acta 57, 2213–2222.

Elthon, D., 1992. Chemical trends in abyssal peridotites-refertilization of depleted suboceanic mantle. J. Geophys. Res. Solid Earth 97, 9015–9025.

Fleet, M.E., Crocket, J.H., Liu, M.H., Stone, W.E., 1999. Laboratory partitioning of platinum-group elements (PGE) and gold with application to magmatic sulfide-PGE deposits. Lithos 47, 127–142.

Fonseca, R.O.C., Campbell, I.H., O'Neill, H.S.C., Fitzgerald, J.D., 2008. Oxygen solubility and speciation in sulphide-rich mattes. Geochim. Cosmochim. Acta 72, 2619–2635.

Frey, F.A., Green, D.H., 1974. Mineralogy, geochemistry and origin of lherzolite inclusions in victorian basanites. Geochim. Cosmochim. Acta 38, 1023–1059.

Gao, S., Rudnick, R.L., Carlson, R.W., McDonough, W.F., Liu, Y.S., 2002. Re–Os evidence for replacement of ancient mantle lithosphere beneath the North China craton. Earth Planet. Sci. Lett. 198, 307–322.

Handler, M.R., Bennett, V.C., 1999. Behaviour of Platinum-group elements in the subcontinental mantle of eastern Australia during variable metasomatism and melt depletion. Geochim. Cosmochim. Acta 63, 3597–3618.

Handler, M.R., Bennett, V.C., Esat, T.M., 1997. The persistence of off-cratonic lithospheric mantle: Os isotopic systematics of variably metasomatised southeast Australian xenoliths. Earth Planet. Sci. Lett. 151, 61–75.

Handler, M.R., Bennett, V.C., Dreibus, G., 1999. Evidence from correlated Ir/Os and Cu/S for late-stage Os mobility in peridotite xenoliths: implications for Re–Os systematics. Geology 27, 75–78.

Hart, S.R., Ravizza, G., 1996. Os partitioning between phases in lherzolite and basalt, isotopic studies of crust–mantle evolution. AGU Monogr. 95, 123–134.

Horan, M.F., Walker, R.J., Morgan, J.W., Grossman, J.N., Rubin, A.E., 2003. Highly siderophile elements in chondrites. Chem. Geol. 196, 5–20.

Klein, F., Bach, W.G., 2009. Fe–Ni–Co–O–S phase relations in peridotite–seawater interactions. J. Petrol. 50, 37–59.

Kullerud, G., Yund, R.A., Moh, G.H., 1969. Phase relation in the Cu–Fe–Ni, Cu–Ni–S and Fe–Ni–S systems. Econ. Geol. 4, 323–343.

Le Roux, V., Bodinier, J.L., Tommasi, A., Alard, O., Dautria, J.M., Vauchez, A., Riches, A.J.V., 2007. The Lherz spinel lherzolite: refertilized rather than pristine mantle. Earth Planet. Sci. Lett. 259, 599–612.

Lee, C.T.A., 2002. Platinum-group element geochemistry of peridotite xenoliths from the Sierra Nevada and the Basin and Range, California. Geochim. Cosmochim. Acta 66, 3987–4005.

Li, C., Barnes, S.J., Makovicky, E., RoseHansen, J., Makovicky, M., 1996. Partitioning of nickel, copper, iridium, rhenium, platinum, and palladium between monosulfide solid solution and sulfide liquid: effects of composition and temperature. Geochim. Cosmochim. Acta 60, 1231–1238.

Liu, R.X., Chen, W.J., Sun, J.Z., Li, D.M., 1992. The K–Ar age and tectonic environment of Cenozoic volcanic rock in China. In: Liu, R.X. (Ed.), The Age and Geochemistry of Cenozoic Volcanic Rock in China. Seismologic Press, Beijing, pp. 1–43. In Chinese.

Liu, C.Z., Snow, J.E., Brugmann, G., Hellebrand, E., Hofmann, A.W., 2009. Non-chondritic HSE budget in Earth's upper mantle evidenced by abyssal peridotites from Gakkel ridge (Arctic Ocean). Earth Planet. Sci. Lett. 283, 122–132.

Lorand, J.P., 1990. Are spinel lherzolite xenoliths representative of the abundance of sulfur in the upper mantle. Geochim. Cosmochim. Acta 54, 1487–1492.

Lorand, J.P., Alard, O., Luguet, A., Keays, R.R., 2003a. Sulfur and selenium systematics of the subcontinental lithospheric mantle: Inferences from the Massif Central xenolith suite (France). Geochim. Cosmochim. Acta 67, 4137–4151.

Lorand, J.P., Reisberg, L., Bedini, R.M., 2003b. Platinum-group elements and melt percolation processes in Sidamo spinel peridotite xenoliths, Ethiopia, East African Rift. Chem. Geol. 196, 57–75.

Lorand, J.P., Luguet, A., Alard, O., 2008a. Platinum-group elements: a new set of key tracers for the earth's interior. Elements 4, 247–252.

Lorand, J.P., Luguet, A., Alard, O., Bezos, A., Meisel, T., 2008b. Abundance and distribution of platinum-group elements in orogenic lherzolites; a case study in a Fontete Rouge lherzolite (French Pyrenees). Chem. Geol. 248, 174–194.

Lorand, J.P., Alard, O., Godard, M., 2009. Platinum-group element signature of the primitive mantle rejuvenated by melt–rock reactions: evidence from Sumail peridotites (Oman Ophiolite). Terra Nova 21, 35–40.

Lorand, J.P., Alard, O., Luguet, A., 2010. Platinum-group element micronuggets and refertilization process in Lherz orogenic peridotite (northeastern Pyrenees, France). Earth Planet. Sci. Lett. 289, 298–310.

Luguet, A., Lorand, J.P., Seyler, M., 2003. Sulfide petrology and highly siderophile element geochemistry of abyssal peridotites: a coupled study of samples from the Kane Fracture Zone (45 degrees W 23 degrees 20 N, MARK Area, Atlantic Ocean). Geochim. Cosmochim. Acta 67, 1553–1570.

Luguet, A., Shirey, S.B., Lorand, J.P., Horan, M.F., Carlson, R.W., 2007. Residual platinum-group minerals from highly depleted harzburgites of the Lherz massif (France) and their role in HSE fractionation of the mantle. Geochim. Cosmochim. Acta 71, 3082–3097.

Ma, J.L., Xu, Y.G., 2004. Petrology and geochemistry of the Cenozoic basalts from Yangyuan of Hebei Province and Datong of Shanxi Province: implications for the deep process in the Western North China Craton. Geochimica 33, 75–88 In Chinese.

McDonough, W.F., Sun, S.S., 1995. The composition of the earth. Chem. Geol. 120, 223–253.

Meisel, T., Walker, R.J., Irving, A.J., Lorand, J.P., 2001. Osmium isotopic compositions of mantle xenoliths: a global perspective. Geochim. Cosmochim. Acta 65, 1311–1323.

Morgan, J.W., Walker, R.J., Brandon, A.D., Horan, M.F., 2001. Siderophile elements in Earth's upper mantle and lunar breccias: data synthesis suggests manifestations of the same late influx. Meteorit. Planet. Sci. 36, 1257–1275.

Mungall, J.E., Hanley, J.J., Arndt, N.T., Debecdelievre, A., 2006. Evidence from meimechites and other low-degree mantle melts for redox controls on mantle–crust fractionation of platinum-group elements. Proc. Natl Acad. Sci. USA 103, 12695–12700.

Pearson, D.G., Irvine, G.J., Ionov, D.A., Boyd, F.R., Dreibus, G.E., 2004. Re–Os isotope systematics and platinum group element fractionation during mantle melt extraction: a study of massif and xenolith peridotite suites. Chem. Geol. 208, 29–59.

Peregoedova, A., Barnes, S.J., Baker, D.R., 2004. The formation of Pt–Ir alloys and Cu–Pd-rich sulfide melts by partial desulfurization of Fe–Ni–Cu sulfides: results of experiments and implications for natural systems. Chem. Geol. 208, 247–264.

Peregoedova, A., Barnes, S.J., Baker, D.R., 2006. An experimental study of mass transfer of platinum-group elements, gold, nickel and copper in sulfur-dominated vapor at magmatic temperatures. Chem. Geol. 235, 59–75.

Puchtel, I.S., Humayun, M., 2000. Platinum group element in Kostomuksha komatiites and basalts: implications for oceanic crust recycling and core–mantle interaction. Geochim. Cosmochim. Acta 64, 4227–4242.

Puchtel, I.S., Walker, R.J., Anhaeusser, C.R., Gruau, G., 2009. Re–Os isotope systematics and HSE abundances of the 3.5 Ga Schapenburg komatiites, South Africa: hydrous melting or prolonged survival of primordial heterogeneities in the mantle? Chem. Geol. 262, 355–369.

Rehkämper, M., Halliday, A.N., Fitton, J.G., Lee, D.C., Wieneke, M., Arndt, N.T., 1999. Ir, Ru, Pt, and Pd in basalts and komatiites: new constraints for the geochemical behavior of the platinum-group elements in the mantle. Geochim. Cosmochim. Acta 63, 3915–3934.

Reisberg, L., Lorand, J.P., 1995. Longevity of sub-continental mantle lithosphere from osmium isotope systematics in orogenic peridotite massifs. Nature 376, 159–162.

Reisberg, L., Zhi, X.C., Lorand, J.P., Wagner, C., Peng, Z.C., Zimmermann, C., 2005. Re–Os and S systematics of spinel peridotite xenoliths from east central China: evidence for contrasting effects of melt percolation. Earth Planet. Sci. Lett. 239, 286–308.

Rudnick, R.L., Shan, G., Ling, W.L., Liu, Y.S., McDonough, W.F., 2004. Petrology and geochemistry of spinel peridotite xenoliths from Hannuoba and Qixia, North China craton. Lithos 77, 609–637.

Saal, A.E., Takazawa, E., Frey, F.A., Shimizu, N., Hart, S.R., 2001. Re–Os isotopes in the Horoman peridotite: evidence for refertilization? J. Petrol. 42, 25–37.

Savard, D., Bédard, L.P., Barnes, S.J., 2006. TCF selenium preconcentration in geological materials for determination at sub-mu gg(-1) with INAA (Se/TCF-INAA). Talanta 70, 566–571.

Shirey, S.B., Walker, R.J., 1998. The Re–Os isotope system in cosmochemistry and high-temperature geochemistry. Annu. Rev. Earth Planet. Sci. 26, 423–500.

Snow, J.E., Schmidt, G., 1998. Constraints on Earth accretion deduced from noble metals in the oceanic mantle. Nature 391, 166–169.

Song, Y., Frey, F.A., 1989. Geochemistry of peridotite xenoliths in basalt from Hannuoba, eastern China—implications for subcontinental mantle heterogeneity. Geochim. Cosmochim. Acta 53, 97–113.

Szabo, C., Bodnar, R.J., 1995. Chemistry and origin of mantle sulfides in spinel peridotite xenoliths from alkaline basaltic lavas, Nograd-Gomor Volcanic Field, northern Hungary and southern Slovakia. Geochim. Cosmochim. Acta 59, 3917–3927.

Volkening, J., Walczyk, T., Heumann, K.G., 1991. Osmium isotope ratio determinations by negative thermal ionization mass-spectrometry. Int. J. Mass Spectrom. Ion Processes 105, 147–159.

Walker, R.J., Shirey, S.B., Hanson, G.N., Rajamani, V., Horan, M.F., 1989. Re–Os, Rb–Sr, and O isotopic systematics of the Archean Kolar Schist Belt, Karnataka, India. Geochim. Cosmochim. Acta 53, 3005–3013.

Wood, S.A., 1987. Thermodynamic calculations of the volatility of the platinum group elements (PGE)—the PGE content of fluids at magmatic temperatures. Geochim. Cosmochim. Acta 51, 3041–3050.

Wulf, A.V., Palme, H., Jochum, K.P., 1995. Fractionation of volatile elements in the early solar-system—evidence from heating experiments on primitive meteorites. Planet. Space Sci. 43, 451–468.

Xu, Y.G., Blusztajn, J., Ma, J.L., Suzuki, K., Liu, J.F., Hart, S.R., 2008. Late Archean to early Proterozoic lithospheric mantle beneath the western North China craton: Sr–Nd–Os isotopes of peridotite xenoliths from Yangyuan and Fansi. Lithos 102, 25–42.

Xu, X.S., Griffin, W.L., O'Reilly, S.Y., Pearson, N.J., Geng, H.Y., Zheng, J.P., 2008. Re–Os isotopes of sulfides in mantle xenoliths from eastern China: progressive modification of lithospheric mantle. Lithos 102, 43–64.

Zhang, H.F., Goldstein, S.L., Zhou, X.H., Sun, M., Cai, Y., 2009. Comprehensive refertilization of lithospheric mantle beneath the North China Craton: further Os–Sr–Nd isotopic constraints. J. Geol. Soc. 166, 249–259.

Zhi, X.C., Song, Y., Frey, F.A., Feng, J.L., Zhai, M.Z., 1990. Geochemistry of Hannuoba basalts, Eastern China—constraints on the origin of continental alkalic and tholeiitic basalt. Chem. Geol. 88, 1–33.

Electronic supplement

Table S1. Average mineral compositions of Yangyuan peridotites analyzed by EPMA

	n	SiO$_2$	TiO$_2$	Al$_2$O$_3$	Cr$_2$O$_3$	FeO	MnO	NiO	MgO	CaO	Na$_2$O	Total
Olivine												
YY-04	8	41.1				8.04	0.10	0.38	50.7			100.4
YY-08	6	41.1				9.72	0.13	0.39	50.3			101.6
YY-09	6	41.1				9.16	0.14	0.37	50.3			101.1
YY-11	5	41.2				9.34	0.12	0.39	50.7			101.7
YY-13	5	40.9				9.16	0.11	0.40	49.9			100.5
YY-22	5	40.7				8.80	0.13	0.39	49.7			99.8
YY-26	4	40.8				9.29	0.11	0.39	50.0			100.6
YY-27	6	40.8				9.95	0.15	0.37	49.7			101.0
YY-51	5	40.8				8.14	0.14	0.39	50.4			99.9
YY-52	5	41.0				9.17	0.15	0.38	50.4			101.1
YY-58	5	41.3				8.59	0.10	0.39	51.2			101.5
YY-60	5	41.0				8.68	0.13	0.39	50.7			100.9
Orthopyroxene												
YY-04	5	55.4	0.03	4.12	0.50	5.39	0.12		33.3	0.75	0.05	99.6
YY-08	5	54.6	0.07	5.19	0.34	6.47	0.15		32.6	0.64	0.03	100.1
YY-09	5	54.3	0.09	5.85	0.42	5.95	0.13		32.3	0.97	0.10	100.1
YY-11	5	54.7	0.10	5.69	0.42	6.09	0.13		32.6	0.87	0.09	100.6
YY-13	5	54.4	0.14	5.58	0.49	5.92	0.12		32.2	0.99	0.09	99.9
YY-22	5	54.3	0.04	5.05	0.46	5.69	0.13		32.6	0.82	0.06	99.2
YY-26	5	54.5	0.08	4.82	0.35	6.16	0.13		32.7	0.61	0.05	99.4
YY-27	5	54.5	0.11	5.40	0.33	6.59	0.14		32.4	0.76	0.05	100.3
YY-51	5	55.2	0.02	3.05	0.60	5.32	0.13		33.0	1.09	0.05	98.4
YY-52	5	54.1	0.09	6.32	0.51	5.92	0.12		31.8	1.26	0.11	100.2
YY-58	5	54.6	0.08	5.89	0.58	5.56	0.12		32.5	1.21	0.14	100.6
YY-60	5	55.4	0.10	3.62	0.53	5.63	0.12		33.4	0.85	0.05	99.7
Clinopyroxene												
YY-04	5	52.8	0.17	4.38	1.32	2.04	0.07		16.2	22.1	1.16	100.2
YY-08	5	51.8	0.28	5.17	0.79	2.68	0.06		15.6	22.3	1.04	99.7
YY-09	5	51.6	0.36	6.36	1.05	2.69	0.08		15.7	20.0	1.57	99.4
YY-11	5	52.2	0.40	6.39	0.95	2.56	0.08		15.7	20.4	1.69	100.3
YY-13	3	51.4	0.55	6.12	1.02	2.68	0.09		15.8	20.2	1.41	99.3
YY-22	5	51.9	0.23	5.37	1.08	2.29	0.08		15.9	21.2	1.26	99.3
YY-26	5	51.6	0.40	5.85	0.89	2.52	0.08		15.2	21.2	1.43	99.1
YY-27	5	51.5	0.58	6.50	0.81	2.91	0.08		14.9	21.1	1.53	99.9
YY-51	5	52.5	0.07	2.87	1.24	2.29	0.09		17.3	21.2	0.76	98.4
YY-52	5	51.5	0.30	6.17	0.92	3.03	0.09		16.4	19.6	1.29	99.3
YY-58	5	52.1	0.30	6.34	1.21	2.73	0.10		16.4	19.5	1.54	100.3
YY-60	5	52.6	0.28	3.75	1.29	2.29	0.08		16.9	21.6	0.98	99.8
Spinel												
YY-04	5	0.03	0.10	45.7	24.2	10.7	0.13	0.26	20.0			101.1
YY-08	5	0.03	0.06	55.3	12.3	11.7	0.11	0.37	20.9			100.9
YY-09	5	0.05	0.14	54.9	13.3	10.7	0.11	0.36	21.6			101.1
YY-11	5	0.04	0.12	54.1	12.5	9.76	0.11	0.32	21.1			98.1
YY-13	4	0.06	0.24	50.8	16.4	11.7	0.13	0.34	20.8			100.4
YY-22	4	0.04	0.07	52.1	16.1	10.3	0.12	0.32	20.9			100.0
YY-26	5	0.02	0.06	55.6	12.8	10.6	0.12	0.35	21.0			100.5
YY-27	5	0.03	0.09	56.5	10.8	11.6	0.11	0.38	21.0			100.5
YY-51	5	0.04	0.15	28.0	39.7	14.0	0.21	0.18	16.9			99.2
YY-52	5	0.07	0.15	51.9	14.8	11.5	0.11	0.35	21.2			100.1
YY-58	5	0.08	0.15	50.7	18.2	10.5	0.12	0.34	21.5			101.6
YY-60	5	0.03	0.35	35.9	32.5	13.3	0.19	0.21	18.3			100.7

Note: Elemental compositions are reported as wt. % of oxides. n represents the number of spot analyses. Minerals were not observed to be chemically zoned.

Table 2S. Os concentrations and isotope compositions of peridotite reference materials.

Sample	Method	n	Os conc. (ppb)	$^{187}Os/^{188}Os$
UB-N	CT-N-TIMS (UMCP)[a]	1	3.95	0.12693
	CT-N-TIMS (UMCP)[b]	4	3.85 ± 0.32	0.12722 ± 38
	CT-N-TIMS (UMCP)[c]	4	3.51 ± 0.12	0.12737 ± 25
	CT-ICP-MS (Chicago)[d]	6	3.72 ± 0.35	-
	HPA-N-TIMS (Leoben)[e]	14	3.85 ± 0.13	0.12780 ± 20
GP-13	CT-N-TIMS (UMCP)[b]	5	3.74 ± 0.11	0.12645 ± 12
	CT-ICP-MS (Chicago)[d]	3	3.70 ± 0.02	-
	CT-N-TIMS (Durham)[f]	8	3.87 ± 0.17	0.1262
	CT-N-TIMS (Durham)[g]	5	3.61 ± 0.12	0.12632±9
	HPA-N-TIMS (Leoben)[e]	7	4.06 ± 0.07	
	HPA-N-TIMS (UMCP)[h]	3	3.3 ± 0.1	0.12644 ± 22

n represents the number of analyses. Uncertainties quoted as $2\sigma_{mean}$ if n>1.

a. This study

b. Puchtel et al., 2008.

c. Becker et al., 2006.

d. Puchtel and Humayun, 2005.
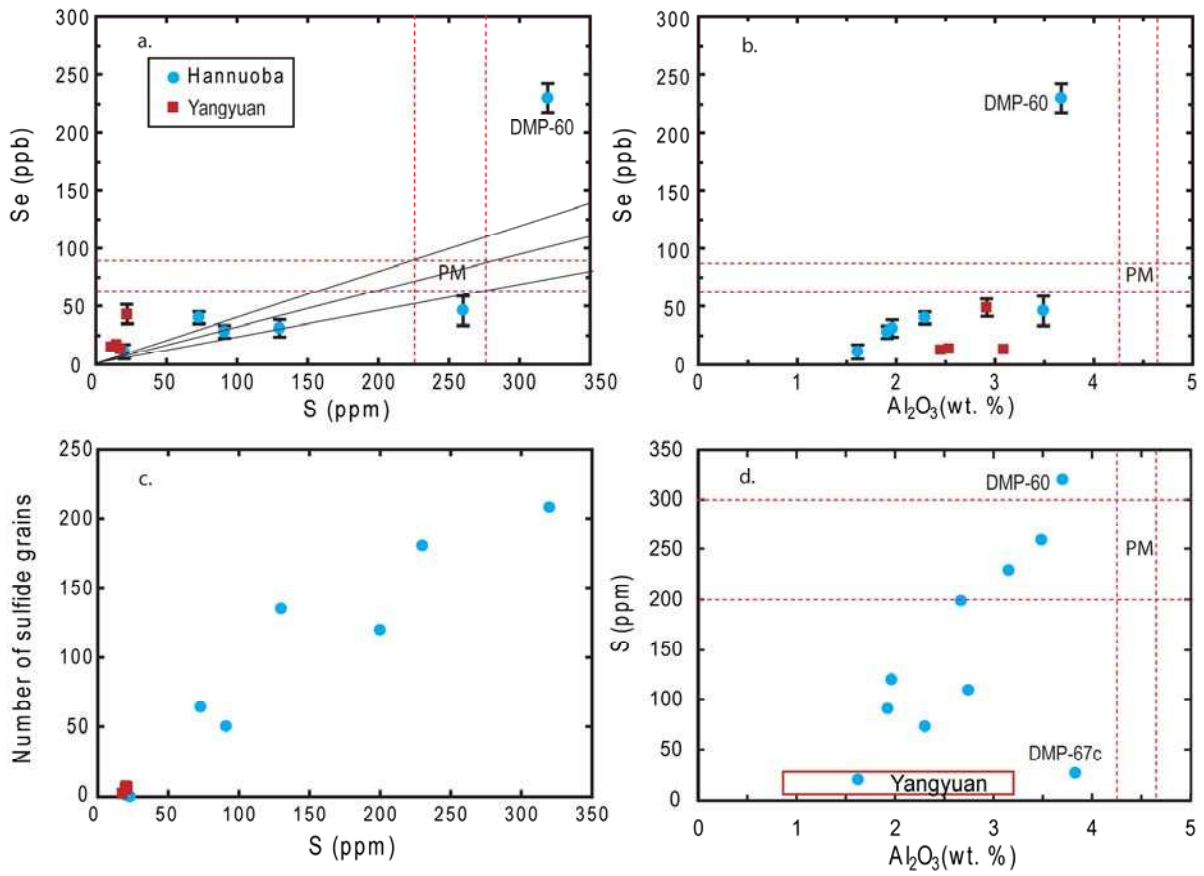
e. Meisel et al., 2003 & Meisel and Moser, 2004.

f. Pearson et al., 2004.

g. Day et al., 2008.

h. James Day, unpublished data.

**Table S3 a and b** is given separately in excel spreadsheets.

Fig. S1

Fig. S1a-d. Plots of (**a**) S vs. Se concentrations, (**b**) Al_2O_3 vs. Se concentrations (**c**) sulfur vs. the number of sulfide grains per thin section and (**d**) S vs. Al_2O_3 concentraitons for Hannuoba and Yangyuan peridotites. PM: primitive mantle (McDonough and Sun, 1995); the solid lines in panel (a) represent the average S/Se ratios (±2σ) of the reference mantle "UM" suite (Morgan et al., 1986); S and Al_2O_3 data of Hannuoba peridotites are from Gao et al. (2002).
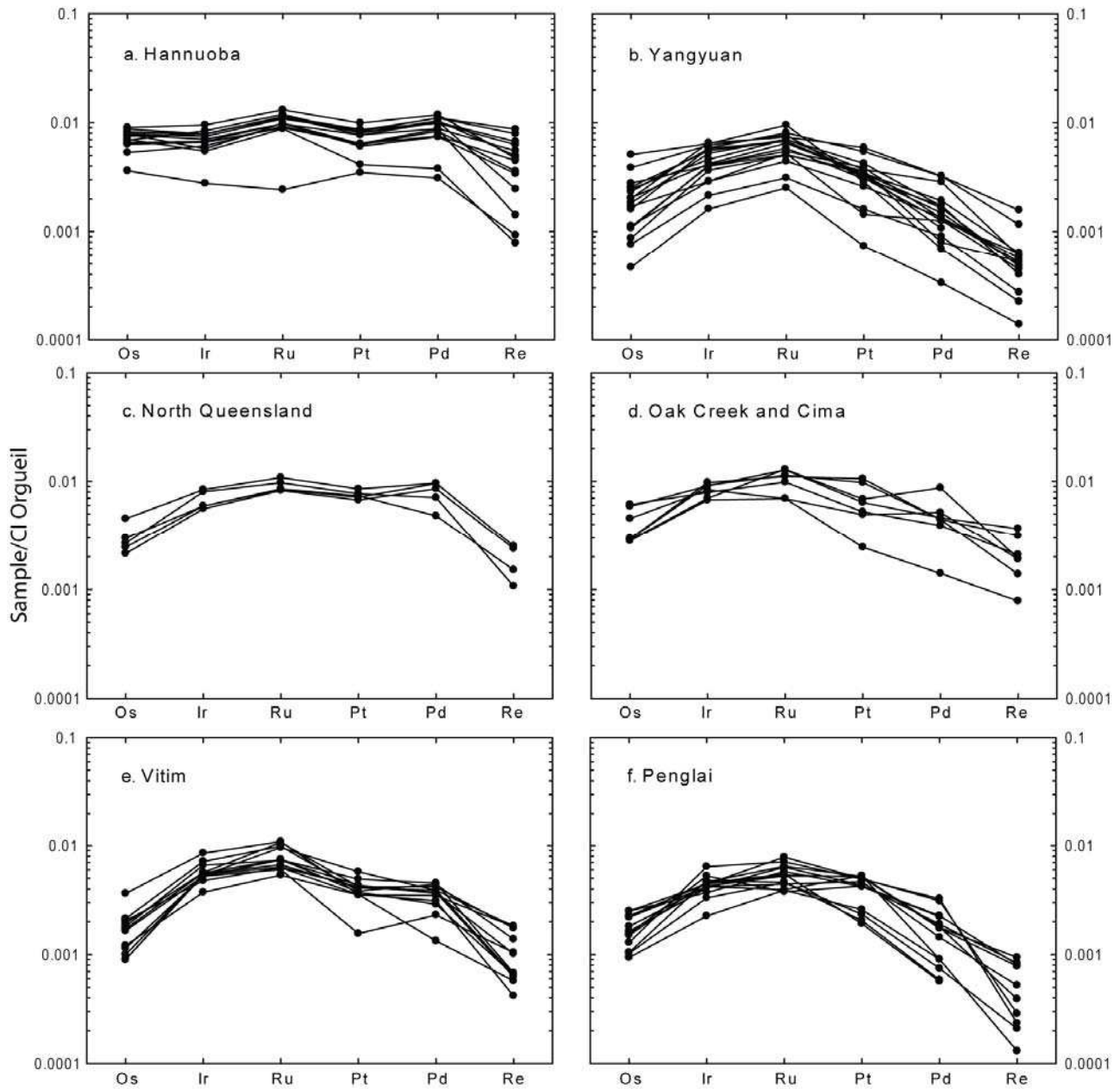
Fig. S2

Fig. S2 a-f. CI chondrite (Orgueil)-normalized patterns for HSE from xenolithic peridotites. **a.** Hannuoba, North China (Becker et al., 2006; this study); **b.** Yangyuan, North China (this study); **c.** North Queensland, Australia (Handler et al., 1999; Handler and Bennett, 1999); **d.** Oak Creek, Sierra Nevada and Cima, Basin and Range (Lee, 2002); **e.** Vitim, Siberia (Pearson et al., 2004); **f.** Penglai, North China Craton (Chu et al., 2009).
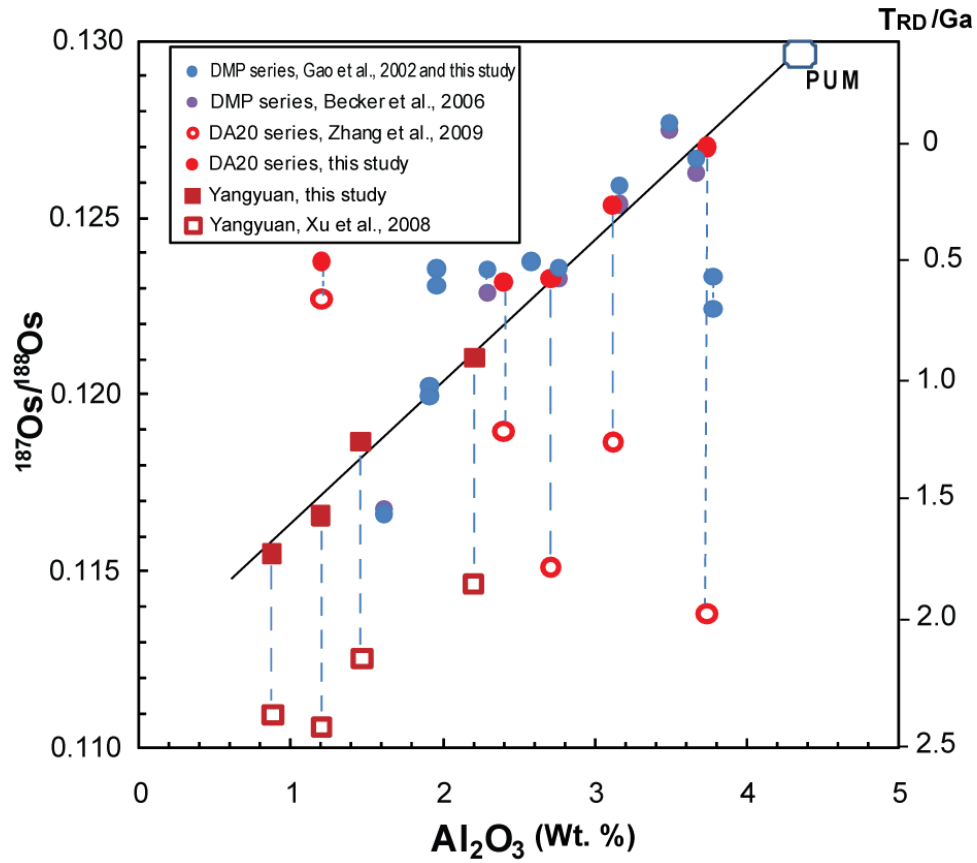
Fig. S3

Fig. S3. Plot of Al_2O_3 vs. $^{187}Os/^{188}Os$ for Hannuoba and Yangyuan peridotites. Data points for the same samples in which $^{187}Os/^{188}Os$ was measured by different methods are connected by a dashed line. The DMP sample series were analyzed by CT-N-TIMS (i.e., Carius tube digestion combined with a negative Thermal Ionization Mass Spectrometry) (Gao et al., 2002; Becker et al., 2006; this study). The DA20 sample series was analyzed by NiS fusion-Os sparging-ICP-MS in the study of Zhang et al. (2009) or and CT-N-TIMS (this study). In addition, three were also measured by HPA (high pressure asher digestion)-N-TIMS. For these three samples, the CT-N-TIMS and HPA-N-TIMS results are indistinguishable. Four Yangyuan samples that were previously measured by NiS-Os sparging-ICP-MS by Xu et al. (2008), were re-analyzed here by CT-NTIMS. PUM: primitive upper mantle (Meisel et al., 2001). The solid line represents the trend defined by the correlation between $^{187}Os/^{188}Os$ and Al_2O_3 for the majority of the samples from both localities.
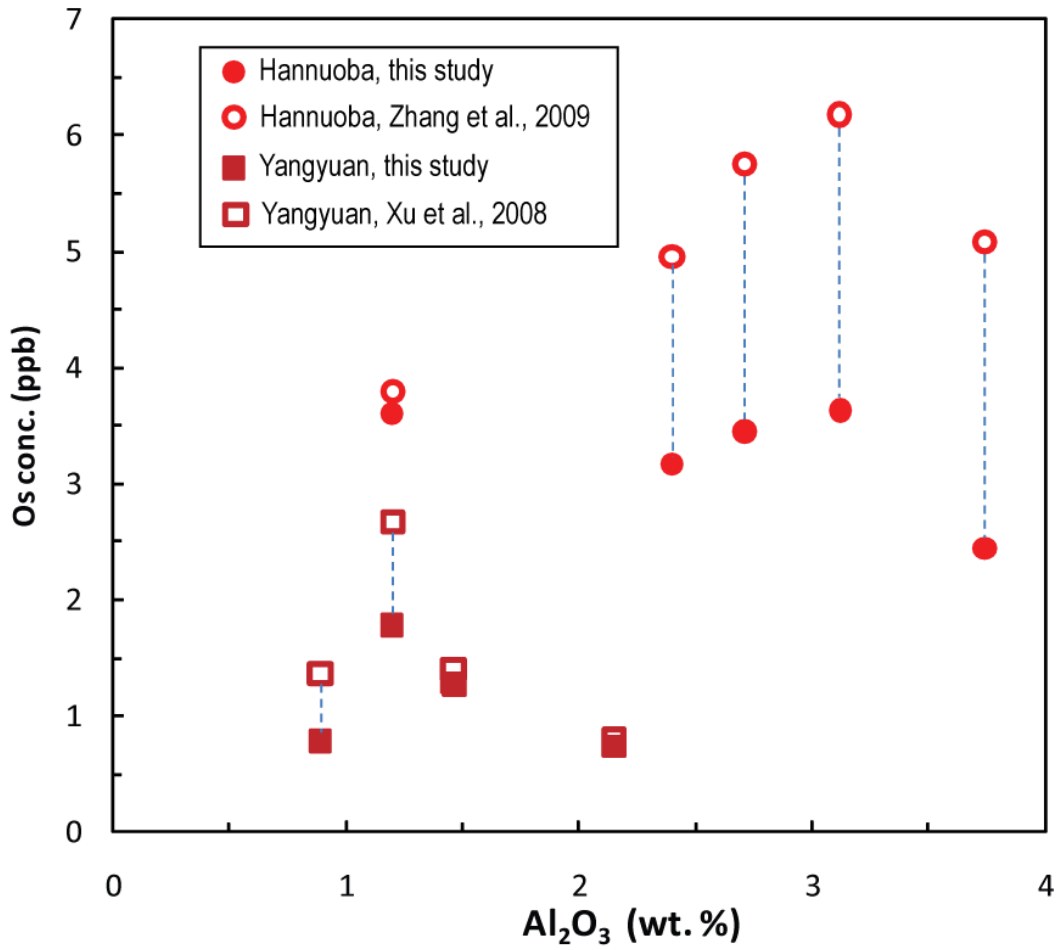
Fig. S4

Fig. S4. Plot of Al_2O_3 vs. Os concentrations of Yangyuan and Hannuoba peridotites that were analyzed by both CT-N-TIMS (this study) and NiS-Os sparging-ICP-MS (Xu et al., 2008; Zhang et al., 2009). The symbols are the same as Fig. S3.

Appendix: Comparison of N-TIMS vs. sparging results

As shown in Table 2 and Figs. 3S and 4S, there are large discrepancies in Os abundances and isotope compositions measured on the same peridotite powders by sparging (Xu et al., 2008; Zhang et al., 2009) versus N-TIMS (this study) for both Yangyuan and Hannuoba samples. The large differences between results affect the model ages for these peridotites and, hence, geodynamic interpretations. Here, we summarize the methods we have taken to assess the accuracy of our data.

In this study, we used the techniques of ID-CT/HPA-N-TIMS: isotope dilution (ID) combined with Carius tube (CT) or high pressure asher (HPA) digestion and measurement by negative thermal ionization mass spectrometry (N-TIMS), the detailed procedures of which are provided in the *Analytical methods* section of our paper (and references therein). By contrast, Xu et al. (2008) and Zhang et al. (2009) employed the NiS fusion-Os sparging-ICP-MS method, the protocol of which is outlined in these two papers and references therein.

In order to compare techniques, we measured four Yangyuan samples from the study of Xu et al. (2008) and five Hannuoba samples from the study of Zhang et al. (2009) by CT-N-TIMS. Three of these five Hannuoba samples were also analyzed by HPA-N-TIMS. In addition, to evaluate the accuracy of our methods, we also measured the peridotite reference material UB-N, which is widely used by the Os isotope, and highly siderophile element (HSE) community. UB-N yielded an Os concentration of 3.95 ppb and $^{187}Os/^{188}Os$ of 0.12693±12 (2σ) using the method of CT-N-TIMS. Both Os concentration and isotope composition of UB-N are well within the range of previously published data (e.g., Meisel et al., 2003; Meisel and Moser, 2004; Puchtel

and Humayun, 2005; Becker et al., 2006; Puchtel et al., 2008) (Table S2). Further, the analyses of the peridotite reference material GP-13 produced identical results for Os abundances and isotopes using CT-N-TIMS versus HPA-N-TIMS techniques in our laboratory (Puchtel et al., 2008; James Day, unpublished data), which are also consistent with results from other labs using similar methods (Meisel and Moser, 2004; Pearson et al., 2004; Day et al., 2008) (Table S2). Likewise, Os isotope compositions and concentrations determined for three Hannuoba peridotites using both CT-NTIMS and HPA-NTIMS methods gave identical results within projected analytical uncertainties (Table 2).

There are substantial discrepancies between our results and those obtained using NiS-Os sparging-ICP-MS (Xu et al., 2008 and Zhang et al., 2009) (Table 2). For Yangyuan peridotites, the Os sparging method by Xu et al. (2008) generated $^{187}Os/^{188}Os$ ratios that are 3.8% to 5.5% (average 4.8%) lower (Fig. S3), and Os concentrations that are 8% to 75% (average 35%) higher (Fig. S4) than our N-TIMS results. Similarly, for Hannuoba peridotites, these numbers are 0.9% to 11.6% (average 5.7%) lower in $^{187}Os/^{188}Os$ (Fig. S3), and 5% to 113% (average 64%) higher in Os concentrations (Fig. S4) when the sparging results of Zhang et al. (2009) are compared to our N-TIMS results. The different mass fractionation corrections (i.e., $^{189}Os/^{188}Os$=1.2212 in Zhang et al. (2009) vs. $^{192}Os/^{188}Os$=3.083 in this study) would only result in very small differences in $^{187}Os/^{188}Os$ (<0.03%) between the labs. These differences in $^{187}Os/^{188}Os$ correspond to 100 to 1500 Ma differences in Os model ages (Fig. 3S). Neither of the previous papers (Xu et al., 2008; Zhang et al., 2009) report sparging data for peridotite reference materials (e.g., UB-N or GP-13) to evaluate the accuracy of the measurements. Zhang et al. (2008) report sparging $^{187}Os/^{188}Os$ results for a highly refractory and serpentinized peridotite from the Mengyin kimberlite (sample F50-9270) that are the same within uncertainty to those reported by

Gao et al. (2002) via N-TIMS and Carius tube digestion. However, Os concentrations exhibited a three-fold difference (3.45 ppb (sparging) vs. 1.20 ppb (N-TIMS), respectively).

In contrast to the data reported by Xu et al. (2008) and Zhang et al. (2009), our new data generally plot along the trend of $^{187}Os/^{188}Os$ and melt depletion indices such as Al_2O_3, defined by previously studied Hannuoba peridotites (DMP series: Gao et al., 2002; Becker et al., 2006; this study) (Fig. 3S). Most importantly for this study, Yangyuan and Hannuoba peridotites have similar distributions of Os model ages (T_{RD}), consistent with their geographic proximity. Although we cannot determine why the sparging method generates such different results, we see no evidence for an Archean or near-Archean component in either locality in our study.

References

Becker, H., Horan, M. F., Walker, R. J., Gao, S., Lorand, J. P., and Rudnick, R. L., 2006. Highly siderophile element composition of the Earth's primitive upper mantle: Constraints from new data on peridotite massifs and xenoliths. Geochimica et Cosmochimica Acta, v. 70, p. 4528-4550.

Chu, Z. Y., Wu, F. Y., Walker, R. J., Rudnick, R. L., Pitcher, L., Puchtel, I. S., Yang, Y. H., and Wilde, S. A., 2009. Temporal Evolution of the Lithospheric Mantle beneath the Eastern North China Craton. Journal of Petrology, v. 50, p. 1857-1898.

Day, J. M. D., Pearson, D. G., and Hulbert, L. J., 2008. Rhenium-osmium isotope and platinum-group element constraints on the origin and evolution of the 1.27 Ga Muskox layered intrusion. Journal of Petrology, v. 49, p. 1255-1295.

Gao, S., Rudnick, R. L., Carlson, R. W., McDonough, W. F., and Liu, Y. S., 2002. Re-Os evidence for replacement of ancient mantle lithosphere beneath the North China craton. Earth and Planetary Science Letters, v. 198, p. 307-322.

Handler, M. R., and Bennett, V. C., 1999. Behaviour of Platinum-group elements in the subcontinental mantle of eastern Australia during variable metasomatism and melt depletion. Geochimica et Cosmochimica Acta, v. 63, p. 3597-3618.

Handler, M. R., Bennett, V. C., and Dreibus, G., 1999. Evidence from correlated Ir/Os and Cu/S for late-stage Os mobility in peridotite xenoliths: Implications for Re-Os systematics. Geology, v. 27, p. 75-78.

Lee, C. T. A., 2002. Platinum-group element geochemistry of peridotite xenoliths from the Sierra Nevada and the Basin and Range, California. Geochimica et Cosmochimica Acta, v. 66, p. 3987-4005.

Mcdonough, W. F., and Sun, S. S., 1995. The Composition of the Earth. Chemical Geology, v. 120, p. 223-253.

Meisel, T., and Moser, J., 2004. Reference materials for geochemical PGE analysis: new analytical data for Ru, Rh, Pd, Os, Ir, Pt and Re by isotope dilution ICP-MS in 11 geological reference materials. Chemical Geology, v. 208, p. 319-338.

Meisel, T., Reisberg, L., Moser, J., Carignan, J., Melcher, F., and Brugmann, G., 2003. Re-Os systematics of UB-N, a serpentinized peridotite reference material (vol 201, pg 161, 2003). Chemical Geology, v. 201, p. 161-179.

Meisel, T., Walker, R. J., Irving, A. J., and Lorand, J. P., 2001. Osmium isotopic compositions of mantle xenoliths: A global perspective. Geochimica et Cosmochimica Acta, v. 65, p. 1311-1323.

Morgan, J. W., 1986. Ultramafic Xenoliths - Clues to Earths Late Accretionary History. Journal of Geophysical Research-Solid Earth and Planets, v. 91, p. 2375-2387.

Pearson, D. G., Irvine, G. J., Ionov, D. A., Boyd, F. R., and Dreibus, G. E., 2004. Re-Os isotope systematics and platinum group element fractionation during mantle melt extraction: a study of massif and xenolith peridotite suites. Chemical Geology, v. 208, p. 29-59.

Puchtel, I. S., and Humayun, M., 2005. Highly siderophile element geochemistry of Os-187-enriched 2.8 ga kostomuksha komatiites, Baltic shield. Geochimica et Cosmochimica Acta, v. 69, p. 1607-1618.

Puchtel, I. S., Walker, R. J., James, O. B., and Kring, D. A., 2008. Osmium isotope and highly siderophile element systematics of lunar impact melt breccias: Implications for the late

accretion history of the Moon and Earth. Geochimica et Cosmochimica Acta, v. 72, p. 3022-3042.

Xu, Y. G., Blusztajn, J., Ma, J. L., Suzuki, K., Liu, J. F., and Hart, S. R., 2008. Late Archean to early proterozoic lithospheric mantle beneath the western North China craton: Sr-Nd-Os isotopes of peridotite xenoliths from Yangyuan and Fansi. Lithos, v. 102, p. 25-42.

Zhang, H. F., Goldstein, S. L., Zhou, X. H., Sun, M., Zheng, J. P., and Cai, Y., 2008. Evolution of subcontinental lithospheric mantle beneath eastern China: Re-Os isotopic evidence from mantle xenoliths in Paleozoic kimberlites and Mesozoic basalts. Contributions to Mineralogy and Petrology, v. 155, p. 271-293.

Zhang, H. F., Goldstein, S. L., Zhou, X. H., Sun, M., and Cai, Y., 2009. Comprehensive refertilization of lithospheric mantle beneath the North China Craton: further Os-Sr-Nd isotopic constraints. Journal of the Geological Society, v. 166, p. 249-259.